Internship project
Unbalanced synchronization of three pendulum clocks

Dynamics and Control
Report number: DC 2017.009

Tutor:	Dr. Jonatan Peña Ramírez	
Msc student	Jasper Maarten Borreman	0779981

TU/e & CICESE - Mechanical Engineering
Ensenada Mexico, 01-09-2016 to 17-11-2016

Abstract

In this work, the synchronous behavior of three pendula coupled through Huygens' coupling is examined analytically, numerically and experimentally. The pendula are transformed into self-sustained oscillators, using a van der Pol torque, which resembles an escapement mechanism of the monumental pendulum clocks used in the experimental analysis. The main objective of this work is to find a new form of asymmetric Huygens' synchronization; specifically searching for the case in which two pendula synchronize in phase, while the third pendulum synchronizes in anti phase with respect to the previous two. The conditions for the existence and stability of the synchronous behavior are determined using the Poincaré method of perturbation. This Poincaré method is modified in order to give the solution for the other synchronous behaviors. Furthermore, using the Poincaré method, the amplitude and phase of predicted synchronous behavior are determined. Finally, the obtained results are compared with computer simulations, and with measurements done with monumental pendulum clocks.

Contents

List of symbols

Symbol	Unit	Property
a	$[-]$	van der Pol factor
α	$[-]$	constant determining the amount of non-linearity in the van der Pol term
b	$[Ns/m]$	damper coefficient
γ	$[rad]$	reference angle of the van der Pol term
f	$[Hz]$	frequency
g	$[m/s^2]$	gravitational acceleration
k	$[N/m]$	spring coefficient
l	$[m]$	length
M	$[kg]$	mass of the rigid beam
m	$[Nms/rad]$	point mass
r	$[rad]$	amplitude
θ	$[rad]$	angle of pendulum
T	$[s]$	period
t	$[s]$	time
τ_c	$[s]$	period elongation
ν	$[-]$	constant determining the amount of non-linearity in the van der Pol term
ϕ	$[rad]$	assumed phase shift
x	$[m]$	horizontal displacement of the carts
ω	$[rad/s]$	angular frequency
z	$[m]$	horizontal displacement
ζ	$[-]$	dimensionless damping coefficient

Chapter 1

Introduction

In the year 1665, Christiaan Huygens made a serendipitous discovery regarding two pendulum clocks, which he had invented [1]. Two clocks, when hung on a common wooden beam, displayed 'sympathetic motion' in the form of antiphase synchronization of their pendula. Upon further investigation it was revealed that the cause of this behaviour were the unobservable vibrations that passed through the wooden beam to which the clocks where attached. Unfortunately for Huygens, the hereafter called Huygens' synchronization did not catch the attention of the scientific community at that time. At the beginning of the 20th century, however, D.J. Korteweg made a simplified linear model that described the motion of the two pendulum clocks. Damping and driving forces were neglegted in this model. With the linear model he predicted that 'other kinds' of sympathy might be possible as well [2].

In recent years, Huygens' synchronization has become a relevant topic for research once more [13–19]. One of the most complete papers about the subject [3] proves the theory of Huygens, using well established physical and mechanical laws. The paper uses a proper modeling of two monumental pendulum clocks and their coupling structure. Using these models, strong analytic proof of in- and anti phase synchronization has been given. Paper [3] furthermore states that multiple forms of synchronization, beside in- and anti phase synchronization, are possible. A recent study [4] shows that it is possible to observe rotating wave solutions in a network of three Huygens' coupled oscillators. Moreover, the aforementioned paper proves the existence of different kinds of synchronizations besides the in- or anti phase behavior.

A remaining uncertainty, however, is if different types of synchronious behaviour exists in a network of three Huygens' coupled oscillators. Understanding and being able to predict alternative forms of synchronization could provide more insight into large Huygens' coupled networks of oscillators. This insight into multiple forms of synchronous behavior of a network consisting of multiple oscillators is very useful since these forms of synchronous behavior are frequently occurring in nature. An example being the multiple biological synchronization inside the human body. Respiration, heartbeat, and blood perfusion rely on synchronization to keep the energy consumption minimal [10]. Seizures, like epilepsy, are abnormal synchronization of neurons and further understanding of these synchronizations could provide solutions that prevent these phenomena [11]. A different example is found in the mechanical field. The placement of two driven unbalanced rotors (like washing machines) on an elastic support can synchronize under certain conditions. These rotors can synchronize in anti phase or in phase [12], providing either significant structural vibration reduction, or undesirable behavior. It is clear that understanding and being able to predict synchronous behavior in large networks could be very beneficial to society, while insufficient knowledge of the subject could bring forth harmful or energy inefficient situations.

This report is organized as follows: Chapter 2 recreates the study done by [4] in order to grasp the Poincaré method of perturbation, and because the model presented in [4] is asymmetrical. This makes the model

perfect for examining other forms of asymmetric Huygens' synchronization.
In Chapter 3, the Poincaré method is used to determine the conditions for existence and stability of in phase and anti phase synchronization, predicting the amplitude and phase of the resulting synchronious behaviour. The solution of each type of synchronous behavior is checked using numerical simulations.
In Chapter 4, additional research is done using a generalized model. Using this model, it can be investigated and shown that asymmetrical anti phase synchronization is a phenomenon that can be observed in a wide range of Huygens' coupled systems.
Chapter 5 contains the results of the experiments that are done using the setup of three Huygens' coupled monumental clocks. Using these results, the validity of the analytic results is examined.
Finally, the findings of this work are concluded and discussed in Chapter 6, providing recommendations for future research where necessary.

Chapter 2

The Poincaré method

First, a short literature study is conducted in order to grasp the Poincaré method of pertubation used to investigate asymmatical antiphase synchronization. The paper of Ramirez and Alvarez [4] provides a useful model for investigating asymmetric synchronization phenomena because the researched standing wave synchronization is an asymmetric form of Huygens' synchronization as well.

2.1 Analytic approach

Paper [4] uses the schematic model shown in Figure 2.1; a rigid beam with mass M $[kg]$ connected to the fixed world with a spring an damper system with coefficients k $[N/m]$ and b $[Ns/m]$, respectively. The beam connects three pendula, with a rigid massless rod of length l_i $[m]$ and point mass m_i $[kg]$. The damping of the pendula are denoted by d_i $[Nms/rad]$, the angle to the vertical axis is denoted by θ_i $[rad]$ and a driving torque u_i is present in order to convert each pendulum into a self-sustained oscillator.

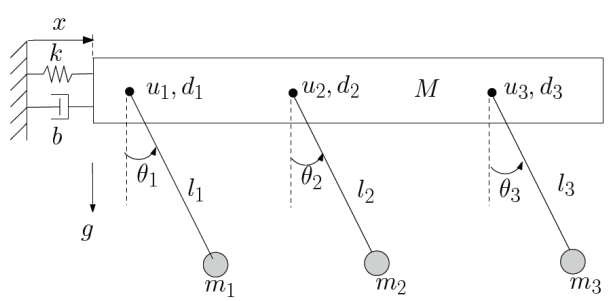

Figure 2.1: *Schematic model of three pendula interacting via Huygens' coupling [4].*

Using the schematic model, the idealized equations of motion can be formed; In this model, the effects of friction have been neglected:

$$
\begin{aligned}
m_i l_i^2 \ddot{\theta}_i &= - m_i l_i \cos\theta_i \ddot{x} - g m_i l_i \sin\theta_i - d_i \dot{\theta}_i + u_i, \\
\left(M + \sum_{i=1}^{3} m_i \right) \ddot{x} &= - kx - b\dot{x} + \sum_{i=1}^{3} m_i l_i \left(\dot{\theta}_i^{\,2} \sin\theta_i - \ddot{\theta}_i \cos\theta_i \right).
\end{aligned} \tag{2.1}
$$

The driving torque u_i, used by the Poincaré method [7,8,17], is designed as a van der Pol term:

$$u_i = \nu(\gamma^2 - \theta_i^2)\dot{\theta}_i, \quad for \quad i = 1, 2, 3. \tag{2.2}$$

In this equation, γ is the reference angle and ν a term which determines the amount of non linearity. The van der Pol term imposes a negative torque on the system if the displacement angle $\theta > \gamma$, halting the pendulum. The term supplies a positive torque to the system if $\theta < \gamma$, resulting in the fact that damping effects do not bring the pendula to a stop and turning them into self sustained oscillators.

The Poincaré method is used in [4] to prove the existence and stability of a standing wave solution, i.e. three identical sinusoidal waves that possess a phase shift with respect to each other. The Poincaré analysis starts by makes four assumptions:

Assumption 1: All pendula are equal, such that $l_i = L$, $m_i = m$, $d_i = d$ for $i = 1, 2, 3$.
Assumption 2: Small angular displacements result in $\sin\theta_i \approx \theta_i$ and $\cos\theta_i \approx 1$.
Assumption 3: The damping and driving force are small, stating that $d = \mu p$, $\nu = \mu c$ with $\mu = \frac{m}{M}$
Assumption 4: All higher order terms of μ^i, $i \geq 2$ are negligible.

Using these assumptions, the equations of motion (2.1), can be linearized and rewritten to:

$$\begin{aligned} \ddot{\theta}_i &= \frac{u_i}{mL^2} - \frac{g}{L}\theta_i - \frac{\ddot{x}}{L} - \frac{d}{mL^2}\dot{\theta}_i, \\ \ddot{x} &= -\frac{k}{M}x - \frac{b}{M}\dot{x} - \mu\sum_{i=1}^{3}\left(\frac{u_i}{mL} - g\theta_i - \frac{d}{mL}\dot{\theta}_i - L\theta_i\dot{\theta}_i^2\right). \end{aligned} \tag{2.3}$$

Finally, equation (2.3) is made dimensionless and simplified by stating that $\tau = \omega t$, $\omega = \sqrt{\frac{g}{L}}$, $q = \frac{kL}{gM}$, $s = \frac{b\sqrt{L}}{M\sqrt{g}}$ and $a = \frac{1}{mL\sqrt{gL}}$. The result is written in matrix form:

$$\frac{d}{d\tau}\begin{bmatrix}\theta_1\\ \dot{\theta}_1\\ \theta_2\\ \dot{\theta}_2\\ \theta_3\\ \dot{\theta}_3\\ y\\ \dot{y}\end{bmatrix} = \begin{bmatrix} 0 & 1 & 0 & 0 & 0 & 0 & 0 & 0\\ -1 & 0 & 0 & 0 & 0 & 0 & q & s\\ 0 & 0 & 0 & 1 & 0 & 0 & 0 & 0\\ 0 & 0 & -1 & 0 & 0 & 0 & q & s\\ 0 & 0 & 0 & 0 & 0 & 1 & 0 & 0\\ 0 & 0 & 0 & 0 & -1 & 0 & q & s\\ 0 & 0 & 0 & 0 & 0 & 0 & 0 & 1\\ 0 & 0 & 0 & 0 & 0 & 0 & -q & -s \end{bmatrix}\begin{bmatrix}\theta_1\\ \dot{\theta}_1\\ \theta_2\\ \dot{\theta}_2\\ \theta_3\\ \dot{\theta}_3\\ y\\ \dot{y}\end{bmatrix} + \mu\begin{bmatrix} 0\\ \alpha\left(c\left(\gamma^2 - \theta_1^2\right) - p\right)\dot{\theta}_1 - \sum_{i=1}^{3}\theta_i(1+\dot{\theta}_i^{\,2})\\ 0\\ \alpha\left(c\left(\gamma^2 - \theta_2^2\right) - p\right)\dot{\theta}_2 - \sum_{i=1}^{3}\theta_i(1+\dot{\theta}_i^{\,2})\\ 0\\ \alpha\left(c\left(\gamma^2 - \theta_3^2\right) - p\right)\dot{\theta}_3 - \sum_{i=1}^{3}\theta_i(1+\dot{\theta}_i^{\,2})\\ 0\\ \sum_{i=1}^{3}\theta_i(1+\dot{\theta}_i^{\,2}) \end{bmatrix}. \tag{2.4}$$

Equation (2.4) can be diagonalized with the use of transformation $\theta = Vz$ for which $\theta := [\theta_1, \theta_2, ..., y, \dot{y}]$, $z := [z_1, z_2, ..., z_7, z_8]$ and V is the matrix of eigenvectors associated to matrix A. Applying this transformation results in:

$$\dot{z}_r = \lambda_r z_r + \mu f_r(z_1, ..., z_8) \tag{2.5}$$

The values of λ_r are assumed to be of the form:

$$\lambda_r = \begin{cases} i\omega & r = 1,3,5, \\ -i\omega & r = 2,4,6, \\ -\frac{s}{2} + \sqrt{\frac{s^2-4q}{2}} & r = 7, \\ -\frac{s}{2} - \sqrt{\frac{s^2-4q}{2}} & r = 8. \end{cases} \tag{2.6}$$

In this equation $\omega = \frac{2\pi}{T} = 1$. Consequently, the general solution of (2.5) is of the form:

$$z^0 = \begin{cases} \alpha_r e^{i\omega t} & r = 1,3,5, \\ \alpha_r e^{-i\omega t} & r = 2,4,6, \\ 0 & r = 7,8. \end{cases} \tag{2.7}$$

In this equation, α_r is a complex constant of the form $\alpha_r = re^{i\phi_i}$, in which ϕ_i is a phase shift. The fact that the solutions must be real provides that $\phi_1 = \phi_2$, $\phi_3 = \phi_4$ and $\phi_5 = \phi_6$. Furthermore, for the case of the standing wave, it can be assumed that all vibrations have an equally large phase shift with respect to each other. Therefore, the following assumption is made: $\phi_1 = 0$, $\phi_3 = -2\pi/3$ and $\phi_5 = -4\pi/3$.

Note that multiple other cases of synchronous behavior can be examined with the same set of equations determined thus far. This can be done by simply providing different assumptions for the phase shifts ϕ_i.

Paper [4] goes on to use the Poincaré method, which states:

Theorem 1. *Periodic solutions with period $T(\mu) = T + \mu\tau_c$ for the autonomous system* (2.5)*, becoming at $\mu = 0$ periodic (period T) solutions* (2.6) *of the fundamental system, i.e system* (2.5) *with $\mu = 0$, can correspond only to such values of constants $\alpha_1, ..., \alpha_6$, which satisfy equations:*

$$Q_r(\alpha_1, ..., \alpha_6) := -\alpha_6 P_r - \alpha_r P_6 = 0, \qquad r = 1,3,5, \tag{2.8}$$

$$Q_r(\alpha_1, ..., \alpha_6) := -\alpha_6 P_r + \alpha_r P_6 = 0, \qquad r = 2,4, \tag{2.9}$$

where

$$P_l(\alpha_1, ..., \alpha_6) = \int_0^{2\pi} f_l(\alpha_1 e^{\lambda_1 t}, ..., \alpha_6 e^{\lambda_6 t}, 0, 0) e^{-\lambda_l t} dt. \tag{2.10}$$

where $l = 1, ..., 6$.

The Poincaré method furthermore states that the roots $\mathcal{X}$ of the characteristic polynomial

$$P(\mathcal{X}) = det\left(\left.\frac{\partial Q}{\partial \alpha}\right|_{\alpha=\alpha^*} + \alpha_6^* \mathcal{X} I \right) = 0, \tag{2.11}$$

should all have negative real parts, and that the period T of the vibration will be elongated by $T^* := T + \mu\tau_c$ where τ_c is given by:

$$\tau_c = -\frac{P_6(\alpha_1^*, ..., \alpha_6^*)}{\lambda_6 \alpha_6^*}. \tag{2.12}$$

The interested reader is referred to papers [7,20,21] for detailed description or proof of Theorem 1 which provides equations (2.8) through (2.10). Using the equations, the set of equations Q_i of [4] have been recreated

and are shown in equation (2.13). In this set of equations, $Q_{2,4}$ are not shown because they are zero.

$$\begin{aligned} Q_1 &= -\frac{\pi r^2(\sqrt{3}i+1)(-c\gamma^2+cr^2+p)}{lm\sqrt{gl}} = 0, \\ Q_3 &= \frac{\pi r^2(\sqrt{3}i+1)(-c\gamma^2+cr^2+p)}{lm\sqrt{gl}} = 0, \\ Q_5 &= \frac{2\pi r^2(-c\gamma^2+cr^2+p)}{lm\sqrt{gl}} = 0. \end{aligned} \tag{2.13}$$

It can easily be seen that a real positive amplitude r exists and is of the form:

$$r = \pm\sqrt{\gamma^2 - \frac{p}{c}}. \tag{2.14}$$

From (2.14) can be seen that r has real solutions for $\gamma^2 > \frac{p}{c}$.

Equation (2.12) gives the period correction for this solution. The correction has been computed to be zero, meaning that the period of the synchronous solution is equal to the period of an uncoupled pendulum. The period of the solution is $T^* := T = 2\pi$.

From the Poincaré equation (2.11) a characteristic polynomial is obtained of the form:

$$p(\mathcal{X}) = a_5\mathcal{X}^5 + a_4\mathcal{X}^4 + a_3\mathcal{X}^3 + a_2\mathcal{X}^2 + a_1\mathcal{X}^1 + a_0. \tag{2.15}$$

If the real parts of the roots of this characteristic polynomial are negative, it can be concluded that the solution is globally stable. Using MATLAB, the coefficients of the equation (2.15) have been computed, though the analytic form of the equation can not be easily displayed due to its substantial size.

2.2 Numerical simulation

Using the values of the setup provided by [4], displayed in Table 2.1, the roots of the characteristic polynomial have been computed to be $\mathcal{X}_1 = -0.8139$, $\mathcal{X}_{2,3} = -0.4046 \pm 0.0041i$ and $\mathcal{X}_{4,5} = -10.6148 \pm 37.4902i$. The roots indicate that the solution is globally stable since all real parts are negative. The predicted solution for the amplitude provided by equation (2.14) of this stable solution is $r = 0.1122$.

Table 2.1: *Parameter values for system*

Pendulum i for $i = 1, 2$	Coupling bar
$m_i = 0.1[Kg]$	$M = 2.5[Kg]$
$d_i = 0.001[Nms/rad]$	$b = 1.42[Ns/m]$
$g = 9.81[m/s^2]$	$k = 150[N/m]$
$L = l_i = 0.125[m]$	
$\gamma = 0.07[-]$	
$\nu = 0.57[kgm^2/rad^3s]$	
Parameter values according to model 2.4	
$\mu = \frac{m}{M} = 0.04$	$q = \frac{kL}{gM} = 0.7645$
$c = \frac{\nu}{\mu} = 14.25$	$s = \frac{v\sqrt{L}}{M\sqrt{g}} = 0.0641$
$p = \frac{d}{\mu} = 0.0250$	

Using Matlab, the system is simulated numerically. Figure 2.2 shows the simulation results of the system with initial conditions $\theta_1 = 0.01\ [rad]$, $\theta_1 = 0\ [rad]$ and $\theta_1 = 0.09\ [rad]$. The top window of the figure shows the angular displacement of the pendula as a function of time, showing the complete simulation. It can be seen that the system converges to the standing wave solution in approximately 25 seconds. The middle window shows the first five seconds of initial transient behavior, and the bottom window shows the final five seconds for which the system is synchronized in a standing wave pattern. The final behavior of the standing wave is observed for a wide range of initial conditions.
Figure 2.3 shows the last two seconds of the simulation in the top window, with the predicted amplitude plotted as horizontal dotted black lines. The predicted amplitude coincides perfectly with the amplitude of the numerically computed solution, suggesting the correctness of the predicted solution using the Poincaré method. The vertical black dotted lines depict the predicted period of $T = \frac{2\pi}{\omega} = 0.710$ which follows from $\omega = \sqrt{\frac{g}{l}}$. As can be seen, the standing wave displays precisely one complete vibration in this interval, showing that no (significant) period elongation is present.
The bottom of Figure 2.3 shows that mechanical vibrations of the connecting beam. It can be seen that the vibrations vanish at the moment the standing wave solution is reached and shows that the final state of the system is reached.

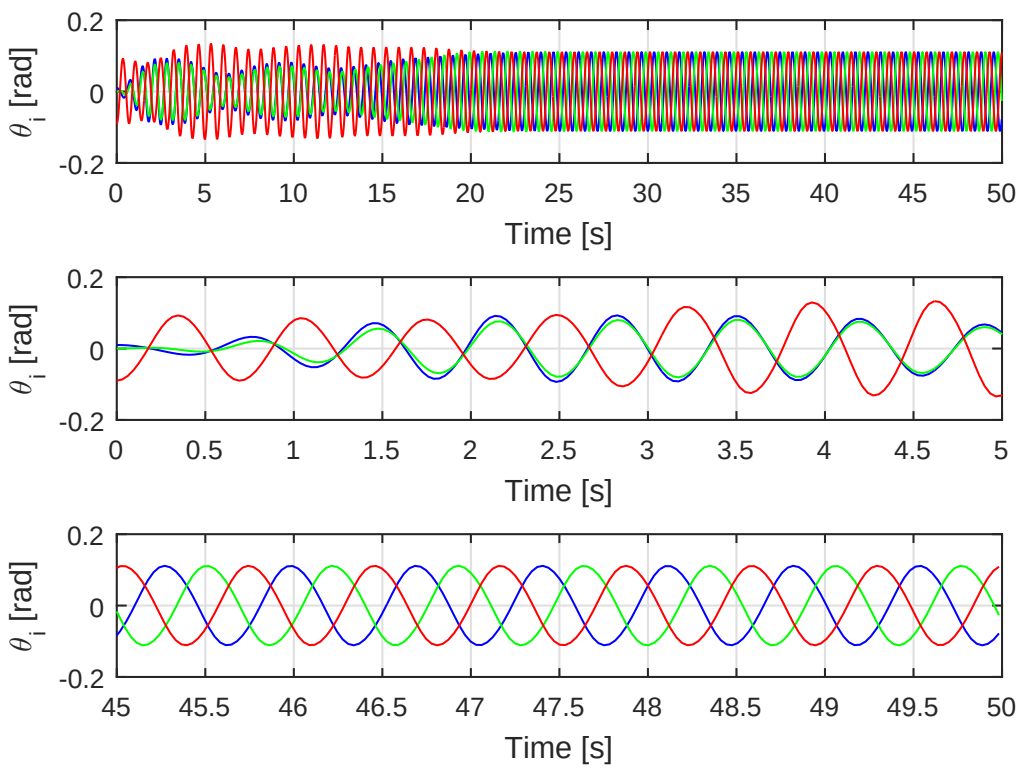

Figure 2.2: *Simulation result of standing wave. On top the complete time series (θ_1 is blue, θ_2 is green and θ_3 is red). The middle figure shows the initial setup behavior, while the bottom shows the final five seconds in which the system has converged to show a standing wave.*

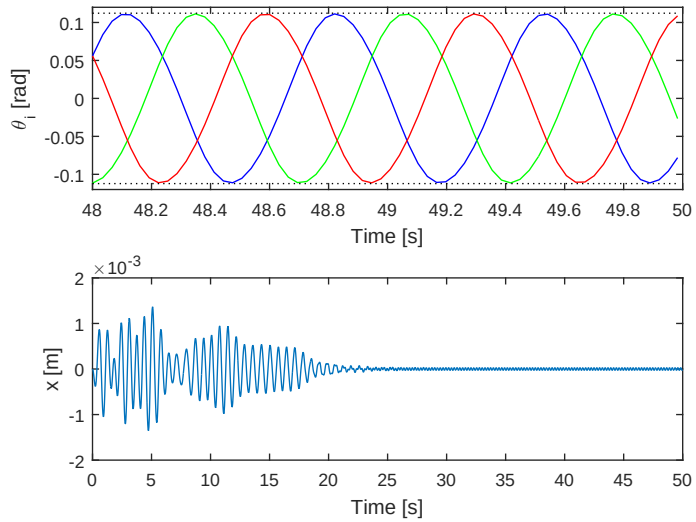

Figure 2.3: *Simulation result of standing wave. On top the final two seconds of the time series. The dotted horizontal and vertical black dotted lines represent the predicted amplitude and period respectively. The bottom figure shows the mechanical vibrations of the coupling beam.*

2.3 Other synchronous behavior

As previously noted, the method used to investigate the standing wave, can easily be adjusted in order to investigate other forms of synchronization by modifying the phase assumption imposed on the complex amplitude of the general solution of equation (2.7). A wide range of phase assumptions has been examined in an attempt to find a new form on synchronization. It has been found that only in phase synchronization provides a solution the the Poincaré equations. In phase synchronization is suggested by assuming that $\phi_1 = \phi_3 = \phi_5 (= 0)$ because no phase difference is present. Using (2.8) through (2.10) once more, the new Q_i equations can be computed:

$$\begin{aligned} Q_{1,3,5} =& 2\pi a r^2(-c\gamma^2 + cr^2 + p) + \frac{6\pi r^2 s(r^2+1)}{q^2 - 2q + s^2 + 1}, \\ Q_{2,4} =& 0. \end{aligned} \tag{2.16}$$

The amplitude of the vibration is found by solving $Q_i = 0$:

$$r = \pm \frac{1}{\sqrt{-ac(q^2 - q + s^2 + 1) - 3s}} \cdot \frac{\sqrt{ac\left(-\gamma^2 q^2 + 2\gamma^2 q - \gamma^2 s^2 - \gamma^2\right) + ap\left(q^2 - 2q + s^2 +\right) + 3s}}{ac\left(q^2 - 2q + s^2 + 1\right) + 3s}. \tag{2.17}$$

One can see from (2.17), however, that this amplitude will be imaginary if γ is too small. Using the values from Table 2.1 and inserting them in equation equation (2.17), results in the necessity that $\gamma > 0.2831$ in order for the amplitude to be real. Using the values from Table 2.1 and equation (2.11), a specific polynomial and its roots are computed:

$$\begin{aligned} \mathcal{X}_1 =& 21 - 266\gamma^2, \\ \mathcal{X}_{2,3} =& 19.0 - 111.0\gamma^2 - 2.6\sqrt{(60\gamma^2 + 9.7)(33\gamma^2 - 17)}, \\ \mathcal{X}_{4,5} =& 19.0 - 111.0\gamma^2 + 2.6\sqrt{(60\gamma^2 + 9.7)(33\gamma^2 - 17)}. \end{aligned} \tag{2.18}$$

Because the real value of all roots need to be negative, this gives that a value of $\gamma > 0.4137$ is needed. Every driving torque value larger than $\gamma \approx 0.1$, however, transforms the vibration in a forced "unnatural" vibration in the numerical simulation.
Changing other pendulum parameters, like the damping of the hinge point, changes equation (2.18) significantly. A crude test, using a range of different sets of variables, has not provided a case in which the numerical analysis matches the computed characteristics using the Poincaré method. The needed driving torque, resulting from the large γ makes the vibration look unnatural in all cases. Appendix A shows an example of a simulation with a high driving torque. The fact that the in phase synchronization can not be proven using the Poincaré method, does not prove it does not exist at all. It is possible, however, that in order to observe the phenomenon, a relatively high driving torque is necessary.

2.4 Chapter summary

In this chapter, the Poincaré method of pertubation has been grasped and used to recreate the results of [4]. Furthermore, the schematic model of Figure 2.1 has been introduced and used to derive the equations of motion needed for the analysis. It has been noted that the Poincaré method can be used to investigate other forms of synchronization by making another assumption for the phase shift. By assuming that all phase shifts ϕ are zero, in phase synchronization has been investigated. From the results of this investigation it could be concluded that a too large driving torque is needed for stability, transforming the vibration into a forced "unnatural" vibration.

Chapter 3

Asymmetric synchronization

3.1 Asymmetric anti phase synchronization

In this section, the standing wave solution of the previous chapter is expanded to obtain a solution for asymmetric anti phase synchronization. This type of synchronization involves two pendulums that swing in phase while the third pendulum will have a motion in exactly the opposite direction. In order to still maintain a balance, however, this implies that the lone pendulum will need either a bigger mass, a bigger amplitude or a more forceful movement. Extensive testing has concluded that a combination of a doubled amplitude in combination with a two times higher driving force on one pendulum, provides a solution. For the other considerations you are referred to Appendix B. The two times higher driving force on the pendulum makes that pendulum have a doubled amplitude. Because of the doubled amplitude, this pendulum supplies enough vibrations to the coupling beam in order to match the doubled mechanical vibrations provided by the pendula swinging in phase. Now the two in phase pendula and the third pendulum, with the double amplitude, have an equal influence on each other and can synchronize in phase or in anti phase. In this section, this solution is explained in more detail.

3.1.1 Analytic approach anti phase synchronization

Giving one of the pendula a larger driving force essentially means that the reference angle γ of the van der Pol equation will differ in one pendulum. This alters the nonlinear part of the dimensionless equation of motion (2.4) to become:

$$\frac{d}{d\tau}\begin{bmatrix}\theta_1\\ \dot{\theta}_1\\ \theta_2\\ \dot{\theta}_2\\ \theta_3\\ \dot{\theta}_3\\ y\\ \dot{y}\end{bmatrix} = \begin{bmatrix} 0 & 1 & 0 & 0 & 0 & 0 & 0 & 0\\ -1 & 0 & 0 & 0 & 0 & 0 & q & s\\ 0 & 0 & 0 & 1 & 0 & 0 & 0 & 0\\ 0 & 0 & -1 & 0 & 0 & 0 & q & s\\ 0 & 0 & 0 & 0 & 0 & 1 & 0 & 0\\ 0 & 0 & 0 & 0 & -1 & 0 & q & s\\ 0 & 0 & 0 & 0 & 0 & 0 & 0 & 1\\ 0 & 0 & 0 & 0 & 0 & 0 & -q & -s \end{bmatrix}\begin{bmatrix}\theta_1\\ \dot{\theta}_1\\ \theta_2\\ \dot{\theta}_2\\ \theta_3\\ \dot{\theta}_3\\ y\\ \dot{y}\end{bmatrix} + \mu\begin{bmatrix} 0\\ \alpha\left(c\left(\gamma_1^2-\theta_1^2\right)-p\right)\dot{\theta}_1 - \sum_{i=1}^{3}\theta_i(1+\dot{\theta}_i^{\,2})\\ 0\\ \alpha\left(c\left(\gamma_2^2-\theta_2^2\right)-p\right)\dot{\theta}_2 - \sum_{i=1}^{3}\theta_i(1+\dot{\theta}_i^{\,2})\\ 0\\ \alpha\left(c\left(\gamma_2^2-\theta_3^2\right)-p\right)\dot{\theta}_3 - \sum_{i=1}^{3}\theta_i(1+\dot{\theta}_i^{\,2})\\ 0\\ \sum_{i=1}^{3}\theta_i(1+\dot{\theta}_i^{\,2}) \end{bmatrix}. \tag{3.1}$$

Because the nonlinear part of equation (3.1) is equal to the nonlinear part of equation (2.4), the eigenvalues are equal to the values depicted in equation (2.6). However, it has been determined that in addition to twice the driving force, one pendulum needs a doubled amplitude as well. The increased amplitude of pendulum one modifies equation (2.7) to become:

$$z^0 = \begin{cases} 2\alpha_r e^{i\omega t} & s = 1, \\ 2\alpha_r e^{-i\omega t} & s = 2, \\ \alpha_r e^{i\omega t} & s = 3, 5, \\ \alpha_r e^{-i\omega t} & s = 4, 6. \\ 0 & s = 7, 8 \end{cases} \tag{3.2}$$

As previously explained, α_r is a complex constant of the form $\alpha_r = re^{i\phi_i}$ with $\phi_1 = \phi_2$, $\phi_3 = \phi_4$ and $\phi_5 = \phi_6$. The values of ϕ_i, however, are different because pendulum one has a shift of exactly π with respect to the other two pendula, resulting in $\phi_1 = \pm\pi$ and $\phi_3 = \phi_5 = 0$.
Using the Poincaré equations (2.8) through (2.10), the equation for Q_i are recomputed:

$$\begin{aligned} Q_1 =& -\frac{\pi a r^2}{2}\left(-5c\gamma^2 + 20cr^2 + 8p\right) + \frac{6\pi r^4(s - q3i + 3i)}{q^2 - 2q + s^2 + 1}, \\ Q_2 =& \frac{3\pi a c r^2}{2}\left(\gamma^2 - 4r^2\right) - \frac{18\pi r^4(s - qi + i)}{q^2 - 2q + s^2 + 1}, \\ Q_{3,5} =& \frac{\pi a r^2}{2}\left(-c\gamma^2 + 4cr^2 + 4p\right) - \frac{12\pi r^4 s}{q^2 - 2q + s^2 + 1}, \\ Q_4 =& \ 0. \end{aligned} \tag{3.3}$$

From the set of equations, no real amplitude r can be found. This is due to the additive terms on the right that contains imaginary components. If system property parameters q and s are within a certain region, however, the set of equations Q_i provide a real amplitude r. Because q and s depend on the system properties, and are therefore manipulable, the conditions imposed on the variables can be imposed relatively easy. After some investigation, which is explained in detail in Appendix B, the values for q and s have been found:

$$q = 1, \qquad s = -\frac{-9c\gamma^2 + 12p}{4acp}. \tag{3.4}$$

Using these conditions a solvable set of of equations Q can be obtained:

$$\begin{aligned} Q_1 =& -\frac{\pi a r^2(-5c\gamma^2 + 8p)(-3c\gamma^2 + 12cr^2 + 4p)}{8p - 6c\gamma^2}, \\ Q_2 =& \frac{3}{2}\pi a c \gamma^2 r^2 + \frac{18\pi a c^2 \gamma^2 r^4}{4p - 3c\gamma^2}, \\ Q_{3,5} =& \frac{\pi a r^2(-c\gamma^2 + 4p)(-3c\gamma^2 + 12cr^2 + 4p)}{8p - 6c\gamma^2}, \\ Q_4 =& \ 0. \end{aligned} \tag{3.5}$$

$$\tag{3.6}$$

For these equations, a real value for the amplitude r can be found:

$$r = \pm\frac{3c\gamma^2 - 4p}{6c}\sqrt{\frac{3c}{3c\gamma^2 - 4p}}. \tag{3.7}$$

The equation shows that r is real if $3c\gamma^2 \geq 4p$.

The characteristic polynomial for the asymmetric anti phase synchronization can be computed using (2.11). However, the symbolic expression of the polynomial can not be shown due to its large size. Poincaré equation (2.12) is used to compute the the period elongation τ_c, which is zero, providing that $T^* := T = 2\pi$.

3.1.2 Numerical simulation anti phase synchronization

Table 4.1 shows the slightly modified parameter values which are necessary to meet the required values for q and s given by equation (3.4). For the chosen values, the roots are computed to be $\mathcal{X}_{1,2} = -147.79$,

Table 3.1: *Parameter values for system*

Pendulum i for $i = 1, 2, 3$	Coupling bar
$m_i = 0.1[Kg]$	$M = 2.5[Kg]$
$d_i = 0.001[Nms/rad]$	$b = 1.42[Kg]$
$g = 9.81[m/s^2]$	$k = 196.2[N/m]$
$L = l_i = 0.125[m]$	
$\gamma_1 = 0.0663[-]$	
$\gamma_2 = \frac{\gamma_1}{\gamma_2} = 0.0332[-]$	
$\nu = 0.57[kgm^2/rad^3s]$	
Parameter values according to model	
$\mu = \frac{m}{M} = 0.04$	$q = \frac{kL}{gM} = 1$
$c = \frac{\nu}{\mu} = 14.25$	$s = \frac{v\sqrt{L}}{M\sqrt{g}} = 0.0641$
$p = \frac{d}{\mu} = 0.0250$	

$\mathcal{X}_3 = -0.3993$, $\mathcal{X}_4 = -0.2845$ end $\mathcal{X}_5 = -0.1513$. From the negative real parts it can be concluded that the solution is globally stable. The system is simulated numerically with initial conditions $\theta_1 = 0.1$ $[rad]$, $\theta_2 = 0.05$ $[rad]$, $\theta_3 = 0$ $[rad]$ and $x = 0$ $[m]$.

Figure 3.1 shows the time series of the numerical simulation. The top window shows the complete time series which stabilizes to a synchronized solution within ten seconds. The middle window shows the initial transient system behavior, and the bottom window shows the last five seconds in which asymmetrical anti phase solution appears. In the bottom window, the red and green line represent the second and third pendula which have coincided to show in phase synchronization. The blue line represents pendulum one, the pendulum with a doubled driving force, which is in anti phase with respect to the other pendula and has twice their amplitude. Figure 3.2 shows the last two seconds of the simulation in the top window, with the predicted amplitude plotted as horizontal dotted black lines. The two predicted amplitudes coincide perfectly with the amplitudes of the numerically computed solution, suggesting the correctness of the predicted solution using the Poincaré method. The horizontal black dotted lines depict the predicted period of $T = \frac{2\pi}{\omega} = 0.710$ which follows from $\omega = \sqrt{\frac{g}{l}}$.

The bottom of Figure 2.3 shows the mechanical vibrations of the connecting beam. It can be seen that the vibrations reduce to show a residual sinusoidal vibration. This is surprising because the system was presumed to resemble the characteristics of a normal anti phase synchronization of two clocks. In this case the residual vibrations go to zero and the pendula seem to be uncoupled. Figure 2.3, however, displays the residual vibrations more commonly seen in in phase synchronization, which might be due to the fact that there is still in phase synchronization present in the system (namely between pendula two and three).

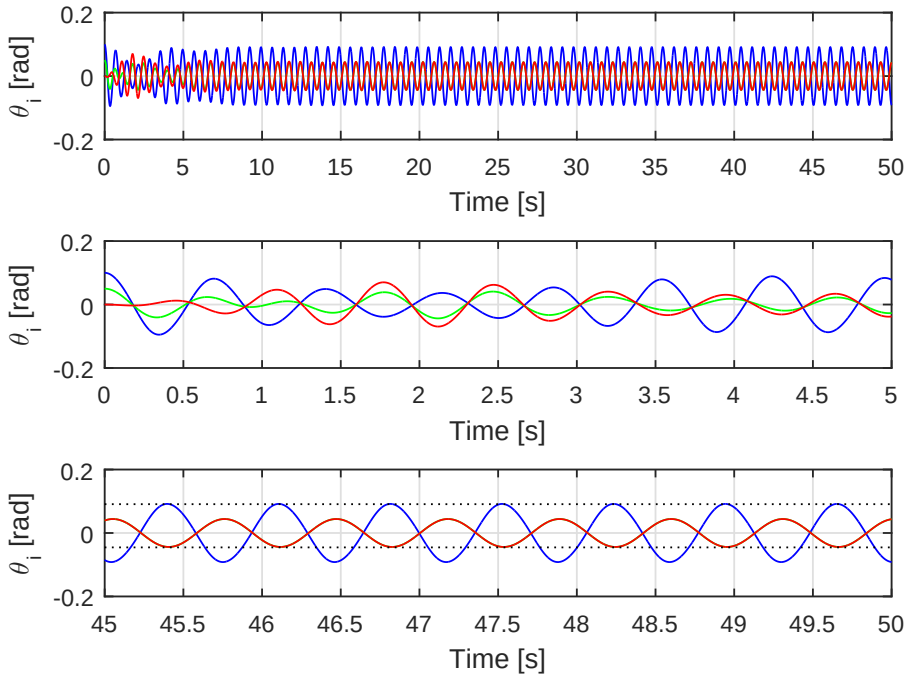

Figure 3.1: *Simulation result of asymmetrical anti phase synchronous behavior. On top the complete time series (θ_1 is blue, θ_2 is green and θ_3 is red). The middle figure shows the initial setup behavior, while the bottom shows the final five seconds in which the system has converged to show anti phase synchronization.*

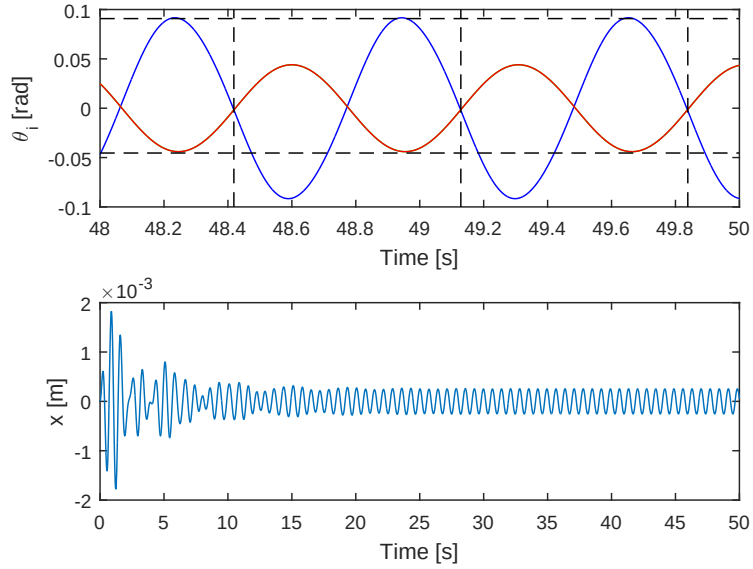

Figure 3.2: *Simulation result of asymmetrical anti phase synchronous behavior. On top the final two seconds of the time series. The dotted horizontal and vertical black dotted lines represent the predicted amplitude and period respectively. The bottom figure shows the mechanical vibrations of the coupling beam.*

3.2 Asymmetric In phase synchronization

Now that the driving torque of one pendulum is doubled, a remaining questing is if in phase synchronization is still possible. For this case, the phase assumptions of $\phi_1 = \phi_3 = \phi_5 = 0$ are chosen once more. The needed amplitude of the pendulum with the doubled driving force is determined by presuming that it is κ times higher than the amplitude of the other pendula. The needed amplitude can now be determined by looking at the resulting Q_2 equation:

$$Q_2 = \pi\kappa acr^4(\kappa^2 - 1) - \frac{\pi r^2 i(\kappa - 1)(\kappa^3 r^2 + \kappa + 2r^2 + 2)}{(1 + s1i - q)} = 0 \tag{3.8}$$

Equation (3.8) can not be solved to give a real amplitude r, giving that $\kappa = 1$ is needed in order to insure that Q_2 is always zero. This gives that the amplitude of the pendulum with the doubled driving force needs to be the same as the other two pendula. Assuming equal amplitudes gives the following Q matrices ($Q_2 = Q_4 = 0$ are omitted):

$$Q_1 = Q_3 = Q_5 = 2\pi apr^2 + \frac{6\pi r^2 s(r^2 + 1)}{q^2 - 2q + s^2 + 1} = 0. \tag{3.9}$$

Because neither $q^2 - 2q + s^2 + 1$ nor s can be negative, it becomes clear that r^2 should be negative in order to solve these equations, giving an imaginary r. This solution suggest that it is not possible to find a set of parameter values for which pure in phase synchronization can be observed. Various numerical simulations have been done in order to verify this. Though some solutions come very close to in phase synchronous solutions, pure in phase synchronization has not been found. Figure 3.3 illustrates the obtained behavior close to in phase. The window on the top left displays the complete time series, and the bottom left window displays the last five seconds of measurement. These two windows would suggest the system shows in phase synchronous behavior. The right window, however, shows a zoom-in of the last peak of the vibration at approximately 499 seconds. It can be seen that there is still a clear phase shift present and no "pure" in phase synchronization is shown. For large simulation times this phase shift remains, suggesting that "pure" in phase synchronization does not exist.

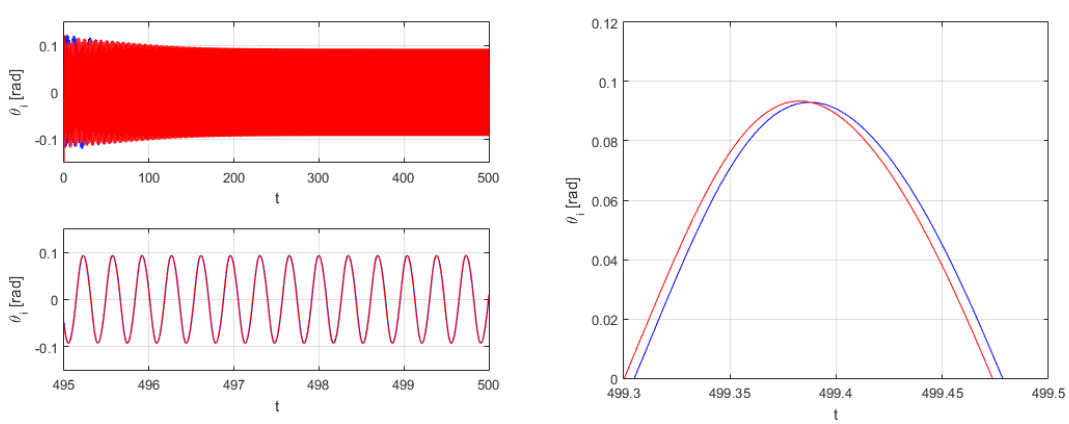

Figure 3.3: *Symulation result of asymmetrical in phase-adjacent behavior. On the top left the compete time series. On the bottom left, a zoom-in of the last five seconds of measurement and on the right a zoom-in of the last peak.*

3.3 Chapter summary

In this chapter, the standing wave solution of Chapter 2 has been expanded to obtain a solution for asymmetric anti phase synchronization. This type of synchronization involves two pendulums that swing in phase while the third pendulum will have a motion in exactly the opposite direction. Extensive testing has concluded that a combination of a doubled amplitude in combination with a two times higher driving force on one pendulum, provides a real amplitude r that can be computed using the Poincaré method. A new dimensionless equation of motion has been made and, using the assumptions for phase shift and amplitude, a new set of equations Q has been derived. By making two additional assumptions for s and q, the set of Q matrices can be solved to find a real amplitude r. Furthermore, using numerical simulations, the correctness of the prediction has been tested, suggesting the correctness of the predicted solution found using the Poincaré method. Finally, the possibility of in phase synchronization for the case in which one pendulum has a two times higher driving force has been investigated. The results using the Poincaré method, as well as the numerical results, have suggested that exact in phase synchronization is not possible.

Chapter 4

Anti phase synchronization in a Huygens' generalized model

As already discussed in the introduction, there are many different situations and models in which Huygens' synchronization can be observed. A coupled pendulum model like Figure 2.1 is among the most popular models used for investigating this phenomena. A more generalized model is shown in Figure 4.1 which has been expanded from a model used in [9]. The figure shows three small carts with a mass m $[kg]$ that are horizontally connected to a rigid structure with spring-damper systems with coefficients κ and β, respectively. The structure of mass m_z $[kg]$ is connected to the fixed world with a spring-damper system with coefficients κ_z and β_z. The complete system and all of the carts are suspended on wheels that are assumed to allow frictionless horizontal movement only. Furthermore, all carts are actuated in order to turn the carts into self-sustained oscillators. The model depicted in Figure 4.1 is a more simple generalized model than the previous model of Figure 2.1, because it contains no conversion from horizontal to rotational forces. Consequently, the cart model of Figure 4.1 could give more insight into the study of Huygens' synchronization.

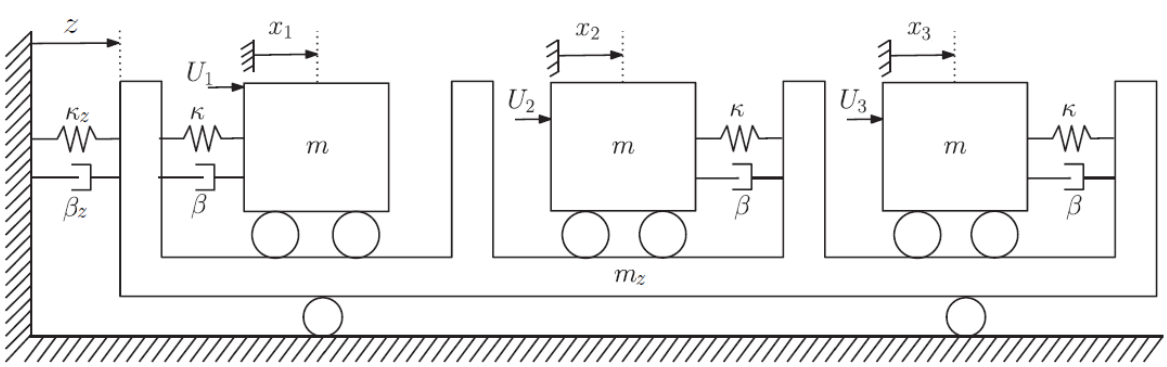

Figure 4.1: *Model of the carts.*

4.1 Analytic approach

The analytic approach starts with forming the idealized equations of motion associated with the model of Figure 4.1:

$$\ddot{x}_i = -\omega^2(x_i - z) - 2\zeta\omega(\dot{x}_i - \dot{z}) - \nu(a_i x_i^2 - i)\dot{x}_i,$$
$$\ddot{z} = -\omega_z^2 z - 2\zeta\omega_z\dot{z} - \mu\sum_{i=1}^{3}(\ddot{x}_i)\,. \tag{4.1}$$

In these equations x_i denotes the displacement of the carts, w and $\zeta = \frac{\beta}{2m\omega}$ the angular eigenfrequency and the dimensionless damping coefficient of the carts, respectively. The terms z, w_z and $\zeta_z = \frac{\beta_z}{2m_z\omega_z}$ are the horzontal displacement, the angular eigenfrequency and the dimensionless damping coefficient of the coupling structure, respectively. The actuation term U_i is designed as van der Pol term $\nu(a_i x_i^2 - 1)\dot{x}_i$. Notice that the van der Pol term is slightly modefied. The new van der Pol term makes use of a factor a instead of a reference angle γ, yielding that energy is supplied to the system if $x_i < \frac{1}{\sqrt{a}}$ and subtracted if $x_i < \frac{1}{\sqrt{a}}$. This form of the van der Pol term, originating form [9], facilitates the interpretation of the obtained results, as will be shown later.
The analysis continues by using the Poincaré method, as has been done in the previous chapters. This gives that the analysis is started by making four assumptions.

Assumption 1: All carts and their (actuated) spring-damper systems are identical.
Assumption 2: Only small displacement are present in the system.
Assumption 3: The damping and driving force terms are small, stating that $2\zeta = \mu d$ and $\frac{\nu}{\omega} = \mu\alpha$ with $\mu = \frac{m}{m_z}$
Assumption 4: All higher order terms of μ^i, $i \geq 2$ are negligible.

Using the four assumptions and and using the dimensionless time $\tau = \omega t$, the equations of (4.1) can be written in dimensionless form. The resulting set of equations are written in matrix form:

$$\frac{d}{d\tau}\begin{bmatrix} x_1 \\ \dot{x_1} \\ x_2 \\ \dot{x_2} \\ x_3 \\ \dot{x_3} \\ z \\ \dot{z} \end{bmatrix} = \begin{bmatrix} 0 & 1 & 0 & 0 & 0 & 0 & 0 & 0 \\ -1 & 0 & 0 & 0 & 0 & 0 & 1 & 0 \\ 0 & 0 & 0 & 1 & 0 & 0 & 0 & 0 \\ 0 & 0 & -1 & 0 & 0 & 0 & 1 & 0 \\ 0 & 0 & 0 & 0 & 0 & 1 & 0 & 0 \\ 0 & 0 & 0 & 0 & -1 & 0 & 1 & 0 \\ 0 & 0 & 0 & 0 & 0 & 0 & 0 & 1 \\ 0 & 0 & 0 & 0 & 0 & 0 & -q & -s \end{bmatrix}\begin{bmatrix} x_1 \\ \dot{x_1} \\ x_2 \\ \dot{x_2} \\ x_3 \\ \dot{x_3} \\ z \\ \dot{z} \end{bmatrix} + \mu\begin{bmatrix} 0 \\ -d(\dot{x_1} - \dot{z}) - \alpha(a_1 x_1^2 - 1)\dot{x_1} \\ 0 \\ -d(\dot{x_2} - \dot{z}) - \alpha(a_2 x_2^2 - 1)\dot{x_2} \\ 0 \\ -d(\dot{x_3} - \dot{z}) - \alpha(a_2 x_3^2 - 1)\dot{x_3} \\ 0 \\ x_1 + x_2 + x_3 - 3z \end{bmatrix}. \tag{4.2}$$

In this equation $q = \frac{\omega_z^2}{\omega^2}$ and $s = \frac{2\zeta_z\omega_z}{\omega}$. Notice that the difference in driving force is modeled in the van der Pol constant a (a_1 for the first cart and a_2 for the second and third cart). The anti phase solution presented in Section 3.1.1 suggests that one cart needs to have twice the amplitude and a doubled driving force. The fact that the driving force scales with $\frac{1}{\sqrt{a_i}}$ would suggest that a ratio $a_2 = 4a_1$ is needed in order to provide a stable solution.

Using the same approach as in Section 3.1.1, it is determined that the eigenvalues λ_r of the system of equation (4.2) are equal to the eigenvalues of equation (2.6). Furthermore, because the same anti phase case is examined, the general solution is equal to that of equation (3.2). In this equation, the complex coefficient α_r is of the form $\alpha_r = re^{i\phi_i}$ with $\phi_1 = \phi_2 = \pm\pi$ and $\phi_3 = \phi_4 = \phi_5 = \phi_6 = 0$.
Using the Poincaré equations (2.8) through (2.10), the equations of Q are computed:

$$
\begin{aligned}
Q_1 &= -2\pi r^2(2d - 2\alpha + 4\alpha a_1 r^2 + \alpha a_2 r^2) &&= 0,\\
Q_2 &= -2\pi\alpha r^4(4a_1 - a_2) &&= 0,\\
Q_{3,5} &= \quad 2\pi r^2(\alpha a_2 r^2 - \alpha + d) &&= 0,\\
Q_4 &= \quad 0 &&= 0.
\end{aligned} \tag{4.3}
$$

The equation (4.3) clearly shows that a nonzero amplitude r is only possible if $a_2 = 4a_1$, concluding that a double driving force of cart one is needed in order to find a solution. Inserting this ratio into equation (4.3) gives: ($Q_2 = Q_4 = 0$ are omitted)

$$
\begin{aligned}
Q_1 &= -4\pi r^2(4\alpha a_1 r^2 - \alpha + d) = 0,\\
Q_{3,5} &= \quad 2\pi r^2(4\alpha a_1 r^2 - \alpha + d) = 0.
\end{aligned} \tag{4.4}
$$

From the set of equations (4.4), a solution for the amplitude r can be found to be:

$$
r = \sqrt{\frac{\alpha - d}{\alpha a_2}} \tag{4.5}
$$

Since r must be real, the condition for the existence of the anti phase synchronization is $\alpha > d$.

Using equation (2.11), the characteristic polynomial for this solution is computed, although its analytic form can not be shown due to its large size. Equation (2.12) is used to compute the the period elongation τ_c, which is zero once more, providing that $T^* := T = 2\pi$.

4.2 Numerical simulation

The values that are considered for the numerical simulation are displayed in Table 4.1. Inserting the values of the table in the computed characteristic polynomial, the roots of the polynomials can be computed to be $\mathcal{X}_1 = -7.067 \cdot 10^{-19} - 1.046 \cdot 10^{-19}i$, $\mathcal{X}_{2,3} = -0.3674 \pm 7.143 \cdot 10^{-12}i$ and $\mathcal{X}_{4,5} = -51.73 \pm -14.45i$. The roots indicate that the solution is globally stable since all real parts are negative.

Note that $\mathcal{X}_1$ is very small ($\mathcal{O}(10^{-19})$). The precision of MATLAB has been altered using the 'digits' function to be more precise. However, no research into the accuracy of this root value has not been done.

The amplitude of this stable solution is computed using equation (4.5), which gives $r = 0.2511$ for cart one and the $r = 0.1255$ for carts two and three.

Table 4.1: *Parameter values for system*

Cart i for $i = 1, 2, 3$	Coupling bar
$m_i = 0.1\ Kg]$	$m_z = 1\ [Kg]$
$\beta = 8 \cdot 10^{-3}\ [Ns/m]$	$\beta_z = 3.2656\ [Ns/m]$
$k = 37.108\ [N/m]$	$k_z = 3.71\ [N/m]$
$\alpha = 0.1\ [-]$	
$a_1 = 37.108\ [-]$	
$a_2 = 148.432\ [-]$	
$d_i = 0.4150\ [-]$	
Parameter values	
$\nu = \alpha\omega\mu = 0.1926\ [kgm^2/rad^3 s]$	$q = \frac{\omega_z^2}{\omega^2} = 1.0475$
$\mu = \frac{m}{M} = 0.01$	$s = \frac{2\zeta_z\omega_z}{\omega} = 0.1695$
$\zeta = \frac{\beta}{2\omega m} = 0.0021$	$\zeta_z = \frac{\beta_z}{2\omega_z m_z} = 0.0828$
$\omega = \sqrt{\frac{k}{m}} = 19.2634$	$\omega_z = \sqrt{\frac{k_z}{m_z}} = 19.7157$

The system is simulated numerically with randomly chosen initial conditions $x_1 = 0.1\ [rad], x_2 = -0.2\ [rad]$, $x_3 = -0.05\ [rad]$ and $z = 0\ [m]$. Figure 4.2 shows the time series of the simulation. The top window shows the complete simulation, while the middle and bottom window show the initial behavior and the "steady" synchronized behavior, respectively. The figure shows that the system reaches its stable anti phase synchronization after a minute, which is longer than the previously simulated systems. This is expected due to the fact that the negative real poles of the characteristic polynomial are close to zero.

Figure 3.2 shows a snippet of the last two seconds of the simulation in the top window. The dotted horizontal lines in the figure depict the amplitudes predicted with the Poincaré method. The vertical dotted lines depict the predicted vibration period T, which can be computed from $\omega = \sqrt{\frac{k}{m}} = 19.2634$, giving $f = \frac{\omega}{2\pi} = 3.0659$ and $T = \frac{1}{f} = 0.3262$. It is clearly visible that the amplitudes and period of the predicted synchronous behavior perfectly coincide with the predicted values suggesting the correctness of the computations.

The bottom window of Figure 4.3 shows the displacement of the rigid coupling structure in the bottom window. The vibrations do not reduce to show a residual sinusoidal vibration, unlike the asymmetrical anti phase simulation of Chapter 3.1.2, but instead asymptotically vanish as long as the anti phase solution is reached. The cause of this difference is unknown and should be researched further.

The fact that the generalized model suggests that asymmetrical anti phase synchronization exists as well, and gives near identical results as provided in Chapter 3.1.2 gives confidence in the fact that anti phase synchronization can be observed in a wide variety of coupled oscillators.

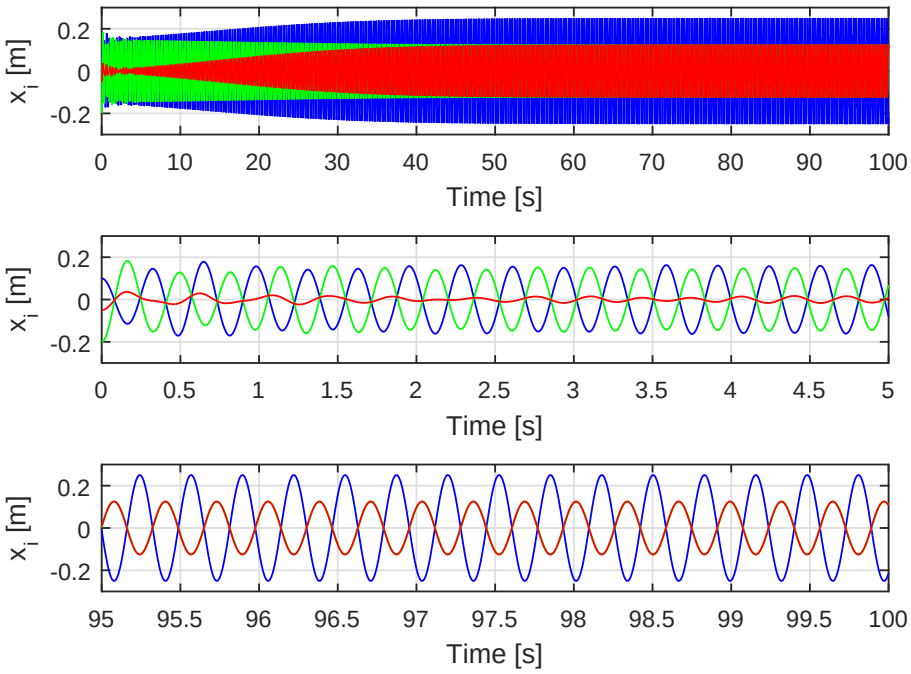

Figure 4.2: *Simulation result of asymmetrical anti phase synchronous behavior. On top the complete time series (θ_1 is blue, θ_2 is green and θ_3 is red). The middle figure shows the initial setup behavior, while the bottom shows the final five seconds in which the system has converged to show anti phase synchronization.*

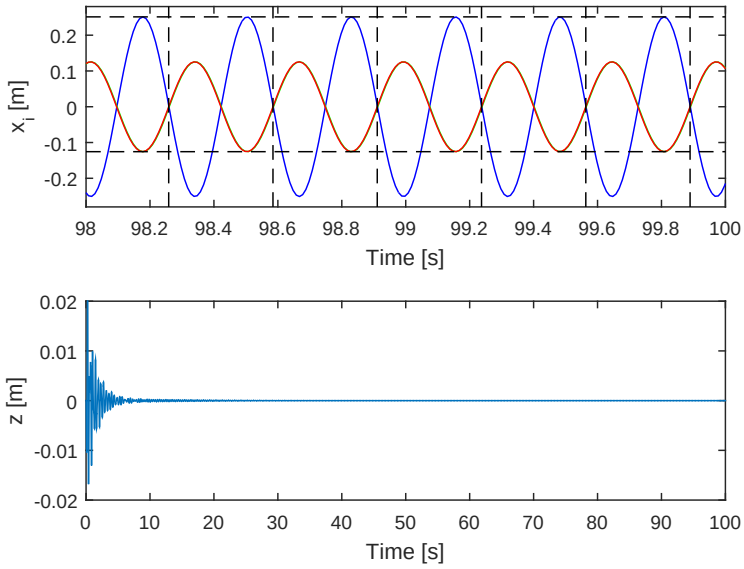

Figure 4.3: *Simulation result of asymmetrical anti phase synchronous behavior. On top the final two seconds of the time series. The dotted horizontal and vertical black dotted lines represent the predicted amplitude and period respectively. The bottom figure shows the mechanical vibrations of the coupling beam.*

4.3 In phase synchronization

As is done in the previous chapter, the existence and conditions for in phase synchronization are investigated. A phase difference of $\phi_1 = \phi_3 = \phi_5 = 0$ is assumed, and using the same method as used in Section 3.2, it has been determined that all amplitudes need to be equal in order to find a real value for the amplitude r. The assumption for phase difference and amplitudes results in a Q_2 equation of:

$$Q_2 = \pi\alpha r^4(a_1 - a_2). \tag{4.6}$$

This equation shows that the doubling of the driving force of one pendulum (resulting from $a_2 = 4a_1$) prevents in phase synchronization. It is clear that $a_1 = a_2$ is needed in order to find a solution. Imposing this condition, essentially stating that all carts are identical, gives (equations $Q_2 = Q_4 = 0$ are omitted):

$$Q_{1,3,5} = 2\pi r^2\left(-\alpha\gamma^2 + \alpha k r^2 + d\right) + \frac{6\pi r^2 s}{q^2 - 2q + s^2 + 1}. \tag{4.7}$$

Solving equation (4.7) results in the expression for the amplitude r:

$$r = \frac{-\sqrt{-\alpha k(-\alpha\gamma^2 + d) - \frac{3\alpha k s}{q^2-2q+s^2+1}}}{\alpha k} \tag{4.8}$$

The roots of the characteristic polynomial and period elongation have been computed using equations (2.8) through (2.10) and are shown in Appendix B.4. The numerical simulation of the in phase solution of the cart model can be found in Appendix B.4 as well. The result of the simulation coincides with the predicted amplitude and period, suggesting the correctness of this solution.

4.4 Chapter summary

In this chapter, the more generalized model of Figure 4.1 has been introduced and investigated in order to give more insight into the study of Huygens' synchronization. Using the model, new equations of motions are derived and the Poincaré method has been used in order to investigate asymmetric anti phase synchronization. Using numerical simulations, the predicted amplitude and period of the Poincareé method have been checked and coincide perfectly. Furthermore, the numerical results of the more generalized model of Figure 4.1 strongly resemble the results found with the use of the model of Figure 2.1. This resemblance has given confidence in the fact that anti phase synchronization can be observed in a wide variety of coupled oscillators. The vibrations of the rigid coupling structure, however, asymptotically vanish for the generalized model. This was not observed in the model of the Huygens' coupled pendulum clocks. The reason of this discrepancy is unknown and should be researched further. Finally, in phase synchronization has been investigated, using the generalized cart model, for which can be concluded that in phase synchronization is possible only if the driving torque is equal for all carts. The computed amplitude and period, determined with the Poincaré method, have been confirmed using numerical simulations.

Chapter 5

Experiments

In this chapter experiments are performed in order to confirm if the previously predicted forms of synchronization are present in three Huygens' coupled pendulum clocks.

5.1 Experimental setup

Figure 5.1 shows the setup of the monumental clocks. The clocks are resting on unsteady supports that are coupled to each other by small wooden beams fixed with clamps. A high-speed camera is placed in front of the clocks, and light blue paper circles are placed on the pendulum weight of each clock. Using image detection software the center of the light blue circles can be detected and their displacement can be tracked. Many of the system parameters, like damping and spring coefficients, are not presently known for

Figure 5.1: *Test setup of three monumental clock using a camera, blue paper and image detection software.*

this setup, while other system parameters are very hard to modify. Provided equipment and time, these system parameters can be identified, though this has not been done for this report. This, however, makes it impossible to predict the amplitudes of the pendula or implement constraints on variables like γ, s and q. Furthermore, a dectable difference is expected between the continuous driving torque of the van der

Pol term and the discontinuous torque given by the escapements mechanism of the clock. Due to the lack of knowledge of system parameters and due to the difference between the modeling of the escapement mechanism and the actual escapement mechanism, comparing the theoretic values for amplitude and period with the measurements obtained with the monumental clock setup, is impossible. The aspiration, therefore, is just to find all forms of synchronization predicted with the Poincaré theory, i.e., the expected results should be qualitatively similar. However, an attempt to double the value for γ is made, by doubling the counter weights of one clock with respect to the other two. The clocks are always initiated close to the investigated synchronous behavior.

5.2 Experimental results with equal γ

For the experiment in which the clocks have equal mechanic weighting, three forms of synchronous behavior has been detected: Anti phase, in phase and standing wave synchronization. Furthermore, forms of pulsating behavior have been observed i.e. vibration wherein the amplitudes of the pendula grow and diminish rapidly in a repeating sequence, showing no definite final form of synchronized behavior. Only the standing wave synchronization appears to be a robust form of synchronization for these types of pendulum clocks.

5.2.1 Anti phase

Figure 5.2 shows the time series of the three Huygens' coupled monumental clocks in which anti synchronization occurs. In the figure, the blue line represents the angle θ_1 of the left pendulum, the green line the angle θ_2 of the middle pendulum and the red black line represent the angle θ_3 of the pendulum on the right. The top of Figure 5.2 shows the the complete time series of the experiment, the middle the intermediary anti phase behavior, and the bottom figure shows the final 35 seconds of the time series. The anti phase depicted by the middle figure appears to be unstable. However, the disappearance of this behavior is actually presumed to be caused by the escapement system of the pendulum clock which needs a minimal displacement of the pendulum of $\theta_i \approx 0.05\ [rad]$ to be engaged. Figure 5.3 shows an enlargement of the time series combined with an extra dotted line displaying the minimum needed displacement in order for the escapement system to remain activated. It can be seen that that at 290 seconds, the two in phase pendula have amplitudes close to the $0.05\ [rad]$ limit, but are still not at half the amplitude of the left pendulum (blue line), which grows to its maximum allowable amplitude of about $0.08\ [rad]$. The amplitude of the other two pendula therefore diminishes to get the proper amplitude ratio, and the right pendulum enters the region where the escapement is no longer engaged. The vibration of the right pendulum reduces to a standstill after which the system tries to start the pendulum up again. The coupled clocks, however, are not able to supply sufficient energy in order for the right pendulum to reach its escapement again. The ending result is always a standstill of one or two pendula.

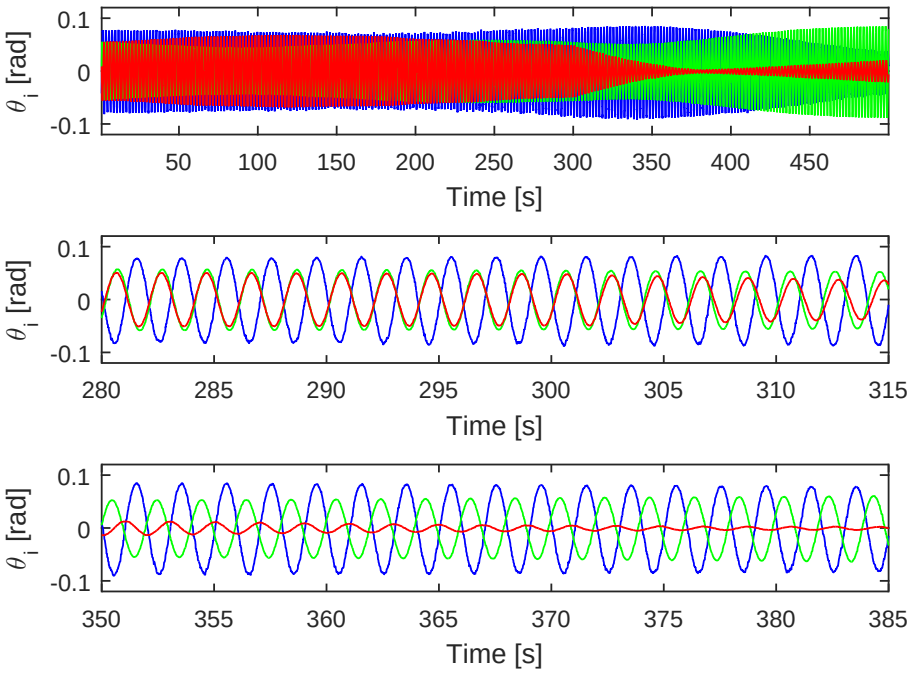

Figure 5.2: *Time series of an experiment showing asymmetrical anti phase synchronization for pendulum clocks with equal γ.*

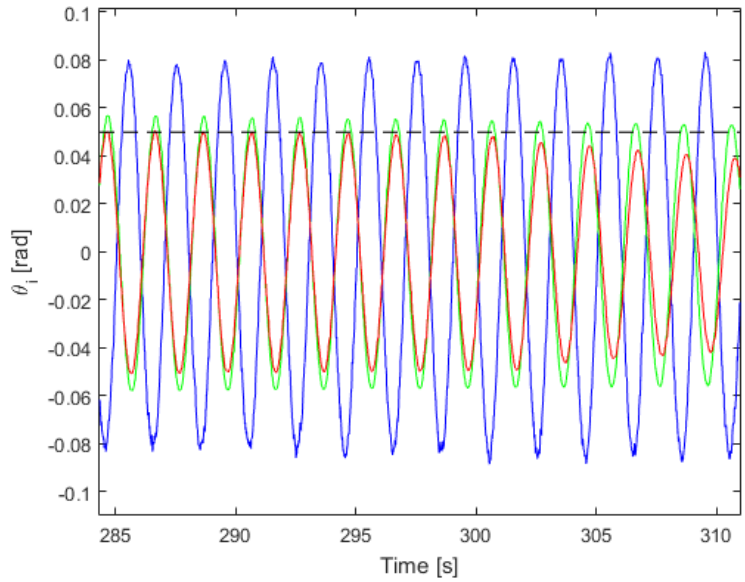

Figure 5.3: *Enlargement of the time series of an experiment showing asymmetrical anti phase synchronization for pendulum clocks with equal γ. The dotted line represents the minimal amplitude for which the escapement mechanism is still engaged.*

5.2.2 In phase

Figure 5.4 show the in phase time series of the three Hugens' coupled clocks. The top window again displays the complete time series, while the middle and bottom figure display the first and last 35 seconds of the experiment, respectively. The figure shows that in phase Hugens' synchronization is possible, though observations suggest that the solution is not as robust as the figure suggest. The behavior only appears if the pendula start close to in phase motion, and small disturbances for the surroundings ultimately results in a stand still of a pendulum or a standing wave.

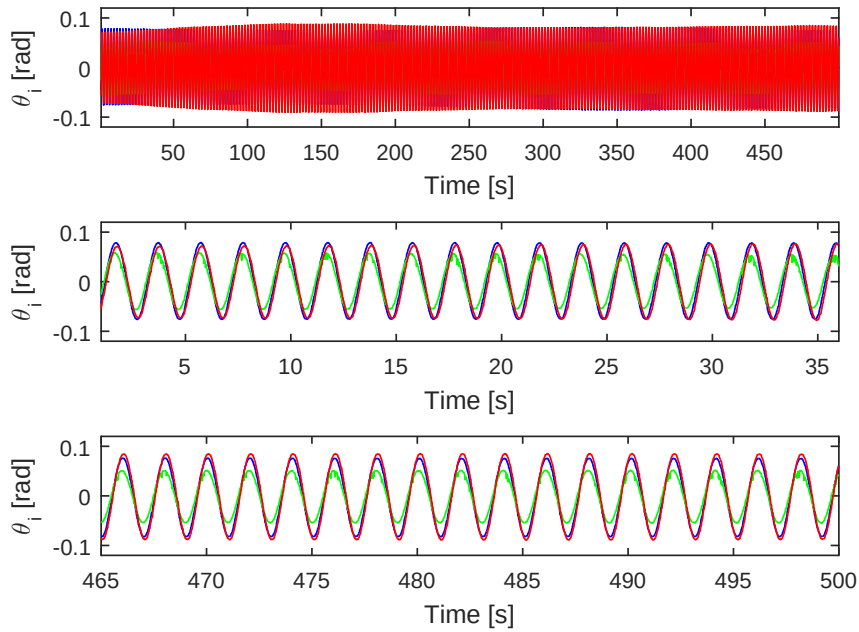

Figure 5.4: *Time series of an experiment showing in phase synchronization for pendulum clocks with equal γ.*

5.2.3 Standing wave

Figure 5.5 shows the time series displaying a standing wave. From top to bottom respectively, the figure shows the complete time series, the first 35 seconds of measurements and the final 35 seconds of measurements. The standing wave synchronization seems to be the most stable synchronization cases solutions, and the only one that does not ultimately result in a stand still of one or two pendula. Furthermore, most initial conditions that were close to the in phase and anti phase case have shown a convergence to a standing wave solution.

5.2.4 Pulsating behavior

As stated before, forms of pulsating behavior have been observed, showing a repetitive pattern of raptly increasing and diminishing amplitudes. Though most of observed kinds of pulsating behavior have resulted in a standstill quite fast, due to the fact than one or more pendula are not engaged by the escapements system at some point, one form has been observed that did not result in a standstill of pendula. Figure 5.6 shows

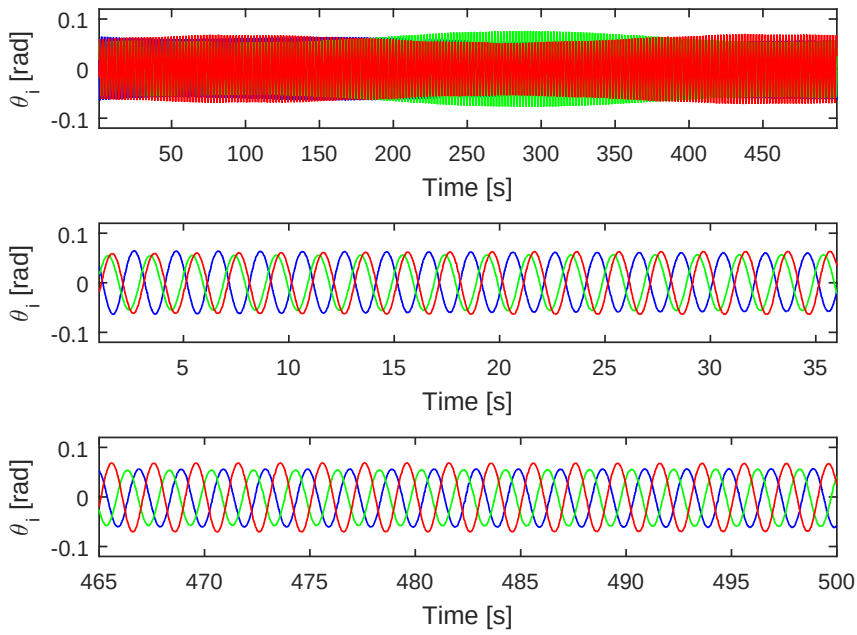

Figure 5.5: *Time series of an experiment showing in phase synchronization for pendulum clocks with equal* γ.

the time series of this pulsating behavior. The top window shows the complete time series while the bottom two windows show snapshots of the different observed behavior.

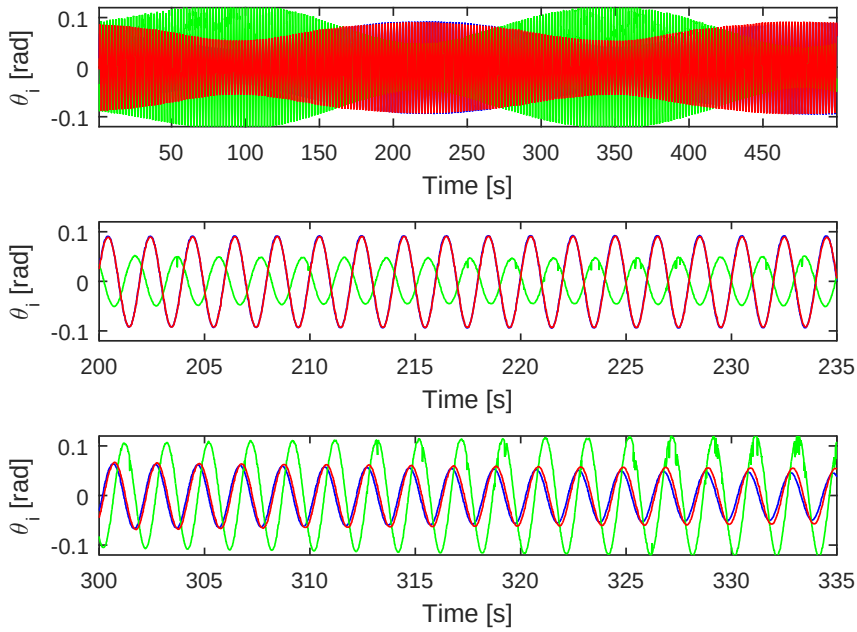

Figure 5.6: *Pulsating behavior experiment with same* γ.

5.3 Experimental results for unequal clocks

An attempt is made to double the driving force term of one of the pendulum clocks, by doubling the mechanical counterweight of one of the monumental clocks. For this system, anti phase and in phase synchronization can be observed. Both forms of synchronization ultimately result in a stand still of one or more pendula. Pulsating behavior and standing wave synchronizations have not been observed.

5.3.1 Anti phase

Figures 5.7a and 5.7b show the time series of the experiment in which the mechanical counterweight of the left monumental clock is doubled. The top windows display the complete time series of the experiments, while the middle and bottom windows display 35 second snapshots of intermediate behavior. Figure 5.7a is initiated in near anti phase motion in which the left pendulum received the same, though negative, initial amplitude as the middle and right pendula. Because the higher driving force on the left pendulum clock, a bigger amplitude could be reached resulting in a longer show of the anti phase synchronization phenomenon. However, this increase of the amplitude of the left pendulum is not enough to be able to keep the middle and right pendulum at a high enough amplitude. In this case, both the middle and right pendulum do not reach their escapement and go to a standstill.

Figure 5.7b is initiated in near anti phase motion in which the right pendulum receives the same, though negative, initial amplitude as the the middle and left pendula. This is done in order to test if the system would favor the clock with the added mechanical weight over the initial conditions. As can be seen in the figure, the system slowly shifts from its inital form of anti phase, to a standing wave of unequal amplitudes ending in an anti-phase synchronization in which the clock with the added mechanical weight has the biggest amplitude. This preference would suggest that only the one form of anti phase synchronization is possibile if one of the clocks has a larger driving force γ that the others. However, Figure 5.7b refutes that statement. The figure shows the time series of the experiment in which the mechanical counterweight of the right monumental clock is doubled. The pendula are initiated in such a way that the right pendulum (red line), with increased driving torque γ, should have the large anti phase amplitude. However, it can be seen in Figure 5.7b that the left pendulum (blue line) grows to display the large anti phase amplitude. This phenomenon was only observed once and has not been reproduced. It is possible that this form of synchronization exists as well, and will most likely not be very robust.

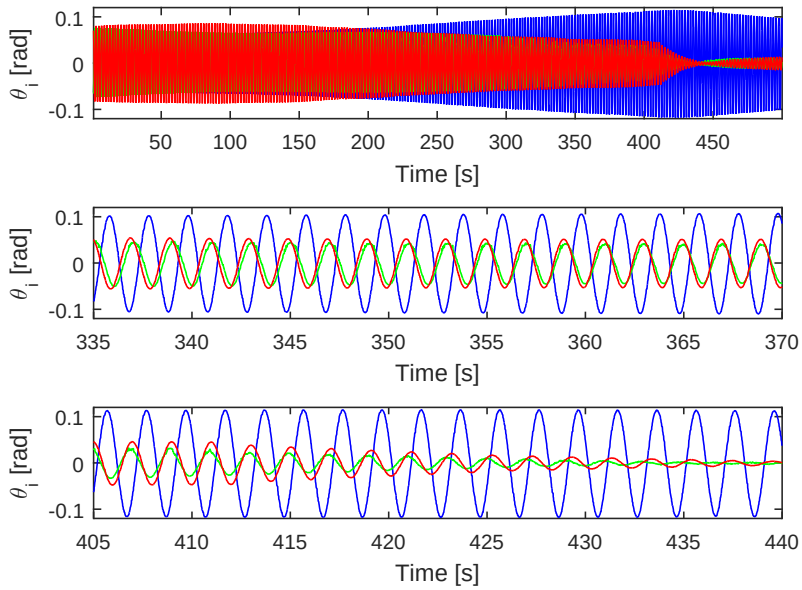

(a) *γ-altered time series displaying anti phase synchronization. The counter weight of the left monumental clock (blue line) is doubled.*

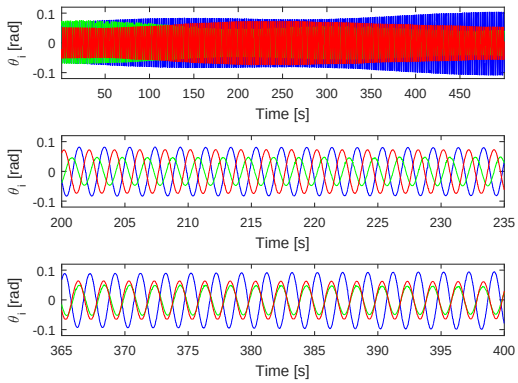

(b) *γ-altered time series displaying anti phase synchronization. The counter weight of the left monumental clock (blue line) is doubled.*

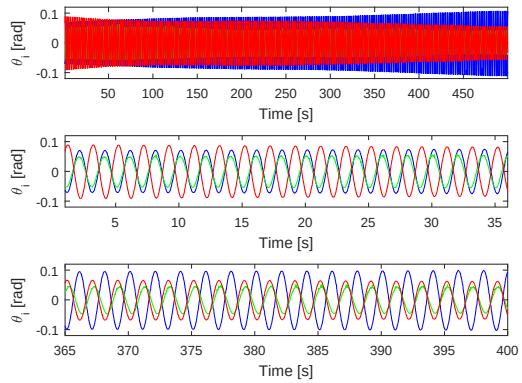

(c) *γ-altered time series displaying anti phase synchronization. The counter weight of the right monumental clock (red line) is doubled.*

Figure 5.7: *Multiple time series of the experiments using the clock setup in which one clock has a doubled mechanical weight.*

5.3.2 In phase

Figure 5.8 shows the time series of the experiment in which the mechanical counterweight of the right (red line) monumental clock is doubled. The middle and bottom window show the first and last 35 seconds of measurement respectively. It can be seen that in phase synchronization is observed with the slight modification that the pendulum of the clock with the added mechanical wight has a slightly higher amplitude and appears to have a light phase lead. This form of synchronization was observed to be quite un robust, behaving the same as the in phase synchronization when all the clocks have the same counter weight.

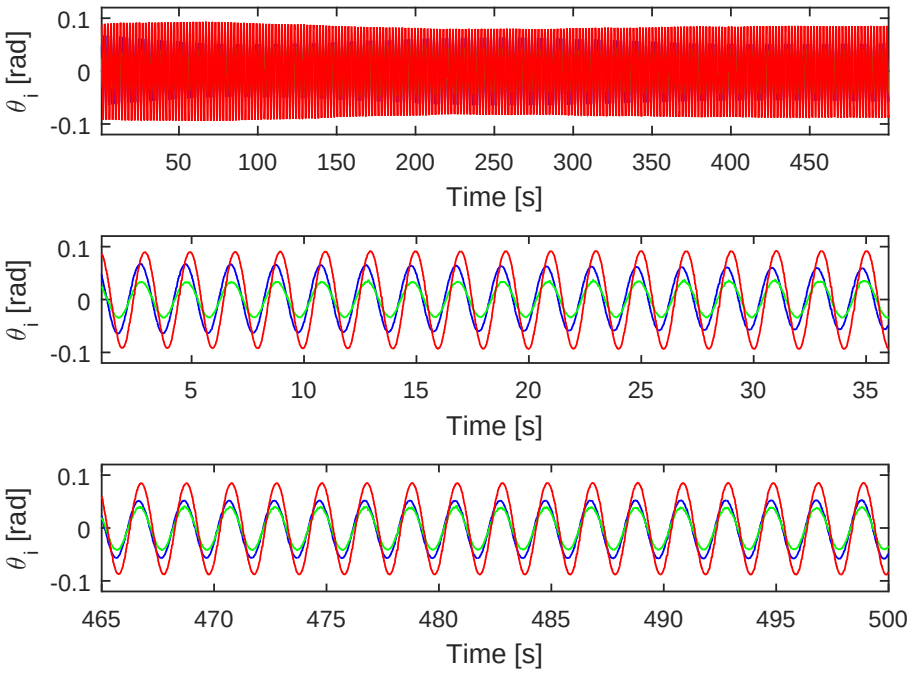

Figure 5.8: *γ-altered time series displaying in phase.*

5.4 Chapter summary

In this chapter, the experimental setup has been introduced an explained. The aspiration of the experiments has been the discovery of all forms of synchronization predicted with the Poincaré method due to a lack of knowledge of the values of the system parameters. However, an attempt has been made to double the value of the driving torque γ by doubling the counter weights of one monumental clock.
For the case in which all clocks are identical, three forms of synchronous behavior have been detected: Anti phase, in phase and standing wave synchronization. Of these forms of synchronization, the standing wave synchronization appeared to be robust, while in- and anti phase synchronization often result in a standstill of one or more pendula. The unstable appearance of the asymmetric anti phase synchronization has been presumed to be caused by the constraints of the setup, which has a maximum and minimum allowable amplitude.
For the case in which the driving torque γ is doubled by increasing the counter weights of one monumental clock, only in- and anti phase synchronization has been observed. Both forms of synchronization did not appear to be robust. However, due to the increase of the maximum amplitude, caused by the doubling of the mechanical weight, the anti phase synchronization can be observed for a longer period of time.

Chapter 6

Conclusions and recommendations

In this chapter the findings of this work are concluded and discussed. Additionally, possible improvements to this research or recommendations for further research are presented.

6.1 Conclusions

In this work, the analytical and numerical results for a standing wave solution of three Huygens' coupled pendula, provided in [4], have been reproduced, and the standing wave synchronization has been observed experimentally in three Huygens' coupled monumental clocks. The standing wave synchronization appears to be stable, as predicted.

Additionally, the Poincaré method used by [4] has been extended in order to prove the existence of asymmetrical anti phase synchronization analytically. The asymmetric solution requires that one pendulum has a double though negative amplitude with respect to the other two pendula, while having a twice as large driving force. Using the Poincaré method, the amplitudes, period length and stability have been predicted and have been confirmed numerically. In practice, asymmetrical anti phase synchronization has been observed, although the experimental setup does not allow the synchronization to exists for an extended period of time. In (almost) identical Huygens' coupled clocks, the synchronization occurs only within a short interval of time. The anti phase synchronization can be observed for a more extended period of time if the driving force of one clock is crudely elevated, which has been done by doubling the mechanical weight of one clock. The double anti phase amplitude is mostly obtained by the clock with the elevated driving force, as was predicted with the theory. One case has been observed, however, in which the double anti phase amplitude was obtained by one of the two other pendula. This can be a coincidence, caused by some form of unknown disturbance, or this is a form of (un robust) synchronization as well.

Furthermore, in phase synchronization of three Huygens coupled pendula with equal driving force has been proven analytically using the Poincaré method. The solution suggests that in phase synchronization is unstable unless a large driving force is applied. Applying this large driving force using numerical simulation, produces an "unnatural" forced vibration, from which no conclusions can be drawn. The numerical simulation, however, appears to produce perfectly stable in phase synchronizations using a lower driving force. During the experiments, in phase synchronization has been observed, although the in phase synchronization does not appear to be robust.

Likewise, for the case in which one pendulum has a doubled driving force, in phase synchronization can not be found using the Poincaré method. This appears to be confirmed by the numerical simulation in which exact synchronization can not be found. The phase synchronization has been observed with the experimental

setup. However, the in phase synchronization did not appear to be robust.

Finally, the Poincaré method has been applied to the more generalized model of Figure 4.1, which is a modification of a model obtained form [9]. The close resemblance of the analytic and numerical results for pendulum model and the generalized cart model suggest that asymmetrical anti phase synchronization is present in a wide range of Huygens' coupled oscillators. A noticeable difference, however, is present between the structural vibrations in the coupling bar. While the pendulum based model shows a small residual sinusoidal vibration, the vibrations of the coupling structure of the card model go to zero asymptotically. The reason for this difference is still unknown.

6.2 Discussion & Recommendation

In the work, some discrepancies have been noticed between the analytically predicted behavior, the computer simulations and the findings during the experiments. Most differences seen in the experiments are due to the fact that the clocks are not identical, as is assumed in both the analytic and numerical parts. This would explain slightly different amplitudes in supposedly identical waves for example. However, other differences between theory and practice are present, resulting in different behavior than initially expected.

The van der Pol term
Although the van der Pol term closely resembles the escapement system of a clock, one big difference can be distinguished. The van der Pol term continuously supplies a negative or positive torque to the system, while the escapement system of a pendulum clock behaves discontinuously by stopping the pendulum and supplying a torque only in a small range of the motion. This explains why during the experiments, a standstill of one or more pendula is a very common phenomenon, while this does not happen during the numerical simulations. A solution to this problem could be the modification of the escapement mechanism of the clocks to one more resembling the van der Pol term, or use a piece-wise continuous function to modeling the escapement mechanism.

The monumental clock setup
A lot of system parameters of the Huygens' coupled monumental clocks are unknown. This makes it almost impossible to modify them to the precise values needed to comply with the restrictions that are predicted to be necessary using the Poincaré method. Additionally, the increase of the driving force has to be done in a very crude manner as well, by doubling the mechanical weight. A study into the exact stiffness, damping and driving force of the monumental clocks, would provide a much better setup. Providing a way to (easily) alter the system parameters could prove useful in later stages of research.
Luckily, the system is already able to show anti phase synchronization, though be it for a short span of time. This is caused by the fact that the escapement system of the clocks is not engaged if a pendulum has half its "normal" amplitude. If the escapement system is altered to allow half the "normal" amplitude, it is assumed that the anti phase synchronization can be observed longer. Finally, the high speed camera measuring system is not without its faults. The high speed camera and its tracking software have given errors often, or lost track of one of the pendula at random times. This is most likely caused by subtle changes of lighting due to the pendula movements, clouds or time of day. The erroneous behavior of the measuring system has made longer measurement times nearly impossible, and many results unreliable. A switch to another form of angle displacement sensor, like the one presented in [6], is preferable.

Difference structural vibrations pendulum- and cart- model
As described at the end of the conclusion, there appears to be a discrepancy between the pendulum model and the more generalized cart model. The reason for the difference between the residual structural vibrations in the models could give more insight into the synchronization phenomenon.

Bibliography

[1] Huygens, C. Correspondance 1664-1665. In Nijhoff, M. (ed.) *Oeuvres complètes de Christiaan Huygens vol. V* (La Societe Hollandaise des Sciences, The Hague, 1893).

[2] Korteweg, D. J. *Les horloges sympathiques de Huygens.* In Nijhoff, M. (ed.) Archives Neerlandaises des Sciences Exactes et Naturelles. vol. XI, 273-295, La Societe Hollandaise des Sciences a Harlem, The Hague, (1906).

[3] Pena Ramirez, J., Olvera, L.A., Nijmeijer, H. and Alvarez, J. (2016), *The sympathy of two pendulum clocks: beyond Huygens' observations.* Sci. Rep. 6, 23580; doi: 10.1038/srep23580

[4] Pena Ramirez, J. and Alvarez, J. (2015), *Rotating waves in oscillators with Huygens' coupling*. In proceedings of the 4th IFAC Conference on Analysis and control of Chaotic systems CHAOS 2015 - Tokyo, Japan, 26-28 August 2015

[5] Pena Ramirez, J., Aihara,K., Fey, R. H. B. and Nijmeijer, H. (2014), *Further understanding of Huygens' coupled clocks: The effect of stiffness.* physica D 270, 11-19

[6] Honeywell, Inc. Technical report (2002) *Applications of magnetic positions sensors* Available at: `http://www51.honeywell.com/aero/common/ documents/Applications-of-Magnetic-Position-Sensors.pdf` (Accessed: September 7, 2016)

[7] Pena Ramirez, J. and Nijmeijer, H. (2015), *The Poincare method: A powerful tool for analyzing synchronization of coupled oscillators.* Indagationes Mathematicae, Available online 27 November 2015, ISSN 0019-3577, `http://www.sciencedirect.com/science/article/pii/S0019357715001056` (Accessed: September 7, 2016)

[8] Blekhman, I. I. (1971), *Synchronization of dynamic systems* (in Russian). Nauka, Moscow.

[9] Pena Ramirez, J., Fey, R.H.B. and Nijmeijer, H. (2013) *Synchronization of weakly nonlinear oscillators with Huygens' coupling*

[10] M. Moser, M. Fruhwirth, and T. Kenner. (2008) *The symphony of life.* Engineering in Medicine and Biology Magazine, IEEE, 27(1): 29-37.

[11] F. Mormann, T. Kreuz, R. G. Andrzejak, P. David, K. Lehnertz, and C. E. Elger. (2003) *Epileptic seizures are preceded by a decrease in synchronization.* Epilepsy Research, 53(3): 173-185

[12] Blekhman I. I. (1988) *Synchronization in science and technology.* ASME Press, New York.

[13] Kanunnikov, A. and Lamper, R. (2003) *Synchronization of pendulum clocks suspended on an elastic beam.* J. Appl. Mech. Tech. Phys. 44, 748-752.

[14] Senator, M. (2006) *Synchronization of two coupled escapement-driven pendulum clocks.* J. Sound Vib. 291, 566-603.

[15] K. Czolczynski, A. Stefanski, P. Perlikowski, and T. Kapitaniak. (2009) *Clustering and synchronization of n Huygens' clocks.* Physica A, 388(24):5013-5023.

[16] R. Dilão. (2009) *Antiphase and in-phase synchronization of nonlinear oscillators: The Huygens' clocks system.* Chaos: An Interdisciplinary Journal of Nonlinear Science, 19(2):023118.

[17] Jovanovic, V. and Koshkin, S. (2012) *Synchronization of Huygens' clocks and the Poincaré method.* J. Sound Vib. 331, 2887-2900.

[18] Pena Ramirez, J. (2013) *Huygens' synchronization of dynamical systems: beyond pendulum clocks* Eindhoven: Technische Universiteit Eindhoven DOI: 10.6100/IR748516

[19] Hoogeboom, F. N. (2015), *Huygens' synchronization: experiments, modeling, and stability analysis.* Master thesis. Eindhoven University of Technology.

[20] A. A. Andronov, A. A. Vitt, and S. E. Khaikin. (1987) *Theory of oscillators.* Dover Publications, New York, 1987.

[21] I. G. Malkin. (1956) *Some problems in the theory of nonlinear oscillations.* State Publishing House of Technical and Theoretical Literature, Moscow, 1956.

Appendix A

The forced vibration

Figure A.1 shows the result of the large γ that the Poincare solution prescribes in order to make the system stable, with a real amplitude. The top figure shows the complete time series, while the middle and bottom window show the first and last five seconds of the simulation respectively. The fact that the system is in phase can not be said to be predicted by the Poincaré method due to the fact that the predicted amplitude and phase do not match the numerical simulation.

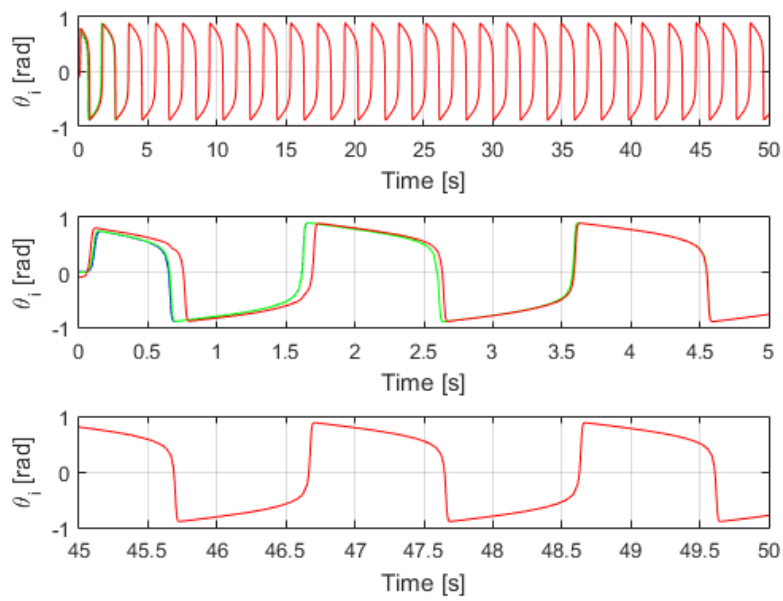

Figure A.1: *Simulation result of the forced vibration as a result of the large γ needed.*

Appendix B

Modifications to the system parameters for observing anti phase synchronization

B.1 Consideration 1; Larger mass of pendulum one

If pendulum one has a larger mass, this alters $m_1 = \epsilon m$, while the other pendulum masses remain $m_{2,3} = m$. Recomputing the dimensionless equation of motion (2.4), the non-linear part of formula (2.4) will change to be as given in equation (B.1). Further computations with this equations does result in a real value of r.

$$\begin{bmatrix} 0 \\ \frac{1}{\epsilon}\left(\alpha\left(c\left(\gamma^2-\theta_1^2\right)-p\right)\dot{\theta}_1\right)-\sum\limits_{i=1}^{3}\theta_i(1+\dot{\theta}_i^{\,2}) \\ 0 \\ \left(\alpha\left(c\left(\gamma^2-\theta_2^2\right)-p\right)\dot{\theta}_2\right)-\sum\limits_{i=1}^{3}\theta_i(1+\dot{\theta}_i^{\,2}) \\ 0 \\ \left(\alpha\left(c\left(\gamma^2-\theta_3^2\right)-p\right)\dot{\theta}_3\right)-\sum\limits_{i=1}^{3}\theta_i(1+\dot{\theta}_i^{\,2}) \\ 0 \\ \sum\limits_{i=1}^{3}\theta_i(1+\dot{\theta}_i^{\,2}) \end{bmatrix} \tag{B.1}$$

It can be seen that an $\frac{1}{\epsilon}$ term multiplies the nonlinear dynamics part of the first pendulum. Using the Poincaré equation, a new set of equation Q can be computed (using a phase difference ϕ_i coherent to the asymmetrical anti phase case). Further computations revealed that for every real value of ϵ, the Q equations do not provide a real value for the amplitude r.

B.2 Consideration 2; Larger displacement of pendulum one

If pendulum one has a larger displacement than the other pendula, c, γ, and p will have to differ. This is determined using the equation for the amplitude r of the standing wave solution displayed in Chapter 2 equation (2.14). Since a bigger amplitude of the pendula could cause problems with the small displacement assumption needed for the linearisation, the amplitude of pendulum two and three are diminished rather than increasing the amplitude of pendulum one. For the case in which the amplitude of pendulum one

is exactly twice the amplitude of pendulum two and pendulum three, this results in a nonlinear part of equations (2.4) shown below. Further computations with this equations result in a set of equations Q, which does not result in a real value of the amplitude r.

$$\begin{bmatrix} 0 \\ \alpha\left(c\left(\gamma^2-\theta_1^2\right)-p\right)\dot{\theta}_1-\sum_{i=1}^{3}\theta_i(1+\dot{\theta}_i^{\,2}) \\ 0 \\ \alpha\left(2c\left((\frac{\gamma}{2})^2-\theta_2^2\right)-\frac{p}{2})\right)\dot{\theta}_2-\sum_{i=1}^{3}\theta_i(1+\dot{\theta}_i^{\,2}) \\ 0 \\ \alpha\left(2c\left((\frac{\gamma}{2})^2-\theta_3^2\right)-\frac{p}{2}\right)\dot{\theta}_3-\sum_{i=1}^{3}\theta_i(1+\dot{\theta}_i^{\,2}) \\ 0 \\ \sum_{i=1}^{3}\theta_i(1+\dot{\theta}_i^{\,2}) \end{bmatrix}. \tag{B.2}$$

B.3 Explanation conditions on q and s

As is explained in Chapter 2, a set of matrices Q has been found which can only be solved to find a real value for the amplitude r, if the system parameters q and s are within a certain range. In this section, a more detailed description is given as to how these ranges are determined. Note that many different tactics for determining the right value for q and s have been tried, though only one solution has been found. Other ranges for q and s,however, might provide a solution as well.

The initial Q equations are shown once more in equation(B.3). The set of equations does not give a real amplitude r.

$$\begin{aligned} Q_1 =& -\frac{\pi a r^2}{2}\left(-5c\gamma^2+20cr^2+8p\right)+\frac{6\pi r^4(s-q3i+3i)}{q^2-2q+s^2+1}, \\ Q_2 =& \frac{3\pi acr^2}{2}\left(\gamma^2-4r^2\right)-\frac{18\pi r^4(s-qi+i)}{q^2-2q+s^2+1}, \\ Q_{3,5} =& \frac{\pi a r^2}{2}\left(-c\gamma^2+4cr^2+4p\right)-\frac{12\pi r^4 s}{q^2-2q+s^2+1}, \\ Q_4 =& \ 0. \end{aligned} \tag{B.3}$$

Notice that imaginary components are present in Q_1 and Q_2 on the right hand side, and are $(s-q3i+3i)$ and $(s-qi+i)$. The value for q is assumed to be $q=1$ in order to cancel this imaginary components. This reduces equation (B.3) to become equation (B.4).

$$\begin{aligned} Q_1 =& -\frac{\pi a r^2}{2}\left(-5c\gamma^2+20cr^2+8p\right)+\frac{6\pi r^4 s}{s^2}, \\ Q_2 =& \frac{3\pi acr^2}{2}\left(\gamma^2-4r^2\right)-\frac{18\pi r^4 s}{s^2}, \\ Q_{3,5} =& \frac{\pi a r^2}{2}\left(-c\gamma^2+4cr^2+4p\right)-\frac{12\pi r^4 s}{s^2}, \\ Q_4 =& \ 0. \end{aligned} \tag{B.4}$$

For this equation a real nonzero amplitude $r_{Q_{3,5}}$ is found by solving $Q_{3,5}=0$. This amplitude $r_{Q_{3,5}}$ is then substituted in equation (B.4). This left nonzero equations for Q_1 and Q_2, which are made zero by choosing

the proper values for parameter $s = -\frac{-9c\gamma^2+12p}{4acp}$. If the values for q and s are substituted in the original set of equation Q, a real positive amplitude r can be found (identical to substituting q and s in $r_{Q_{3,5}}$).

B.4 Figures in phase synchronization of cart model

The values that are considered for the numerical in phase simulation are displayed in Table 4.1. Inserting the values of the table in the computed characteristic polynomial, the roots of the polynomials can be computed to be $\mathcal{X}_1 = -22.1120$, $\mathcal{X}_{2,3} = -10.0421 \pm 8.4392i$ and $\mathcal{X}_{4,5} = -10.0421 \pm 8.4392i$. The roots indicate that the solution is globally stable since all real parts are negative. The amplitude of this stable solution is computed using equation (4.8), which gives an amplitude of $r = 0.0596$ for all carts since all amplitudes have previously been determined to be equal.

The system is simulated numerically with initial conditions close to the in phase solution; $x_1 = 0.1\ [rad]$, $x_2 = 0.05\ [rad]$, $x_3 = 0.03\ [rad]$ and $z = 0\ [m]$. Figure B.1 shows the time series of the simulation. The top window shows the complete simulation, while the middle and bottom window show the initial behavior and the "steady" synchronized behavior, respectively. Figure B.2 shows a snippet of the last two seconds of the simulation in the top window. The dotted horizontal lines in the figure depict the amplitudes predicted with the Poincaré method, while the vertical dotted lines depict the predicted vibration period T. It is clearly visible that the amplitudes and period of the predicted synchronous behavior perfectly coincide with the predicted values suggesting the correctness of the computations.
The bottom window of Figure B.2 shows the displacement of the rigid coupling structure in the bottom window. The vibrations reduce to show a residual sinusoidal vibration.

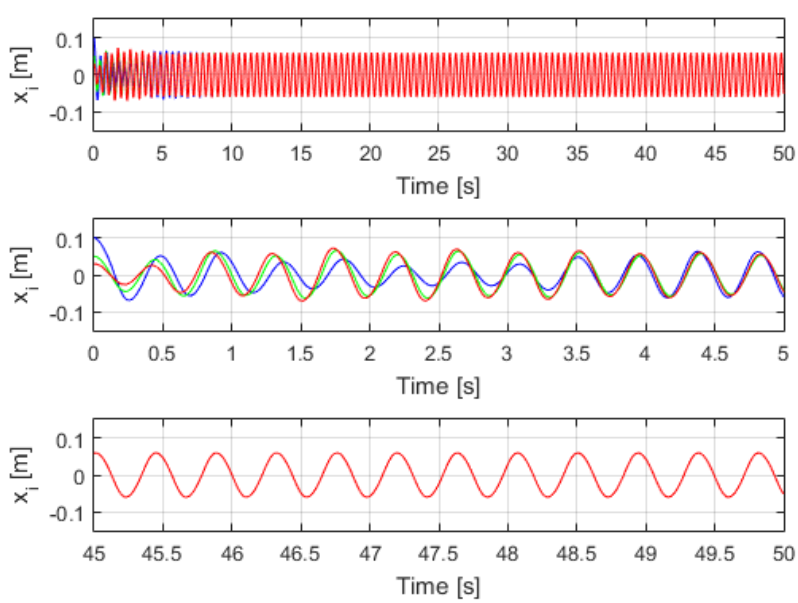

Figure B.1: *Simulation result of asymmetrical anti phase synchronous behavior. On top the complete time series (θ_1 is blue, θ_2 is green and θ_3 is red). The middle figure shows the initial setup behavior, while the bottom shows the final five seconds in which the system has converged to show anti phase synchronization.*

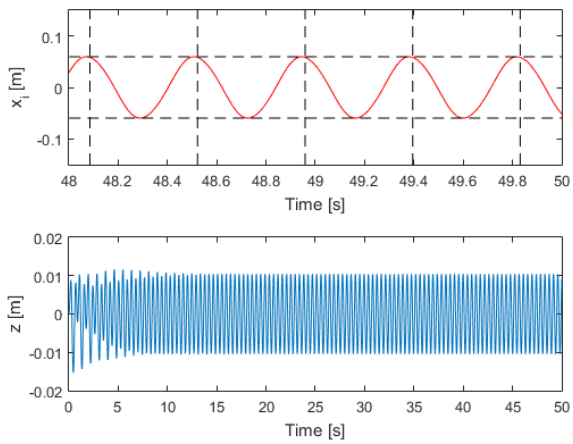

Figure B.2: *Simulation result of asymmetrical anti phase synchronous behavior. On top the final two seconds of the time series. The dotted horizontal and vertical black dotted lines represent the predicted amplitude and period respectively. The bottom figure shows the mechanical vibrations of the coupling beam.*